Three ways of abolishing automaticity in sinoatrial node: ionic modeling and nonlinear dynamics

MICHAEL R. GUEVARA AND HABO J. JONGSMA
Department of Physiology, McGill University, Montreal, Quebec H3G 1Y6, Canada; and Physiological Laboratory, University of Amsterdam, 1105 AZ Amsterdam, The Netherlands

Guevara, Michael R., and Habo J. Jongsma. Three ways of abolishing automaticity in sinoatrial node: ionic modeling and nonlinear dynamics. *Am. J. Physiol.* 262 (*Heart Circ. Physiol.* 31): H1268–H1286, 1992.—A review of the experimental literature reveals that there are essentially three qualitatively different ways in which spontaneous activity in the sinoatrial node can be abolished. We show that these three ways also occur in an ionic model of space-clamped nodal membrane. In one of these three ways, injection of a current pulse abolishes ("annihilates") spontaneous action potential generation. In the other two ways, as some parameter is changed, one sees a sequence of qualitative changes in the behavior of the membrane as it is brought to quiescence. In one of these two ways there are incrementing prepotentials intermixed with action potentials, with a maintained small-amplitude subthreshold oscillation being the limiting case of such behavior. Thus both experimental and modeling work indicate that the number of ways in which spontaneous activity can be abolished, or initiated, in the sinoatrial node is limited. The classification into three ways is based on ideas drawn from the qualitative theory of differential equations, which are introduced. The classification scheme can be extended to encompass behaviors seen in other cardiac oscillators.

annihilation; single-pulse triggering; afterpotentials; delayed afterdepolarizations; subthreshold oscillations; oscillatory prepotentials; bifurcations; chaos

ONE CAUSE of the potentially life-threatening cardiac arrhythmia called sinoatrial arrest is the cessation of spontaneous action potential generation in the sinoatrial node (SAN), the principal natural pacemaker of the mammalian heart. In a search of the literature we have turned up many traces of the transmembrane potential showing cessation of spontaneous activity in the SAN as the result of some experimental intervention. Perusal of these recordings has led us to classify these tracings into three groups, showing that there are essentially three qualitatively different ways in which the normal spontaneous activity of the node can be abolished. In the first way, there is a gradual progressive decline in the amplitude of the action potential until quiescence occurs. In the second way, injection of a brief stimulus pulse annihilates spontaneous activity, which can then be restarted or triggered by injecting a second stimulus pulse. In the third way, before the membrane becomes quiescent as the result of some intervention that gradually takes hold, one sees skipped-beat runs in which spontaneously occurring action potentials are preceded by one or more small-amplitude subthreshold oscillatory prepotentials.

Because all the traces mentioned come from experiments carried out on isolated right atrial preparations or on small pieces of tissue isolated from the SAN, the extent to which the behaviors seen might be accounted for solely by membrane properties of SAN cells is uncertain. For example, subthreshold deflections resembling pre- or afterpotentials recorded in one cell might actually be electrotonic potentials reflecting occurrence of block of propagation into that area of the SAN (10, 44). To avoid this complication in the interpretation of the results, we carried out simulations using an ionic model of an isopotential patch of membrane, where spatial factors of this sort cannot occur. In addition, numerical investigation of an ionic model allows one to probe the ionic basis underlying the particular behavior observed.

The model of isopotential SAN membrane studied here is that of Irisawa and Noma (36). Because it is a Hodgkin-Huxley-type model, it is formulated as a system of nonlinear ordinary differential equations. A major point of this paper is that a branch of nonlinear mathematics, bifurcation theory, can be used to obtain significant insights into qualitative aspects of the various behaviors displayed by this class of model. Indeed, it is our claim that one cannot fully appreciate the results of the numerical simulations presented below and the corresponding experimental findings without also at least a passing acquaintance with concepts stemming from the qualitative theory of differential equations. We therefore interweave presentation of the results of numerical simulation of the model with interpretations of those simulations in terms of the qualitative dynamics of the system. For readers wishing to obtain further details about bifurcation theory, the qualitative theory of differential equations, and related aspects of nonlinear mathematics, several textbooks that are readable by someone with a biological sciences background are now available (1, 25, 71, 74, 84).

METHODS

We investigated the effect of changing, one at a time, many different parameters in the Irisawa-Noma (36) ionic model of isopotential SAN membrane. In several instances, when a parameter was altered sufficiently from its normal value, termination of spontaneous activity resulted. The Irisawa-Noma model is based on voltage-clamp data recorded from small pieces of tissue taken from the rabbit SAN and provides a quantitative description of five currents: the fast inward sodium current (I_{Na}), the slow inward calcium current (I_s), the delayed rectifier potassium current (I_K), the hyperpolarization-acti-

vated pacemaker current (I_h; commonly termed I_f), and a time-independent leakage current (I_l). We used two different methods of investigation, direct numerical integration of the equations and bifurcation analysis.

Numerical integration. We numerically integrated the Irisawa-Noma equations in a manner identical to that employed in a recent study that showed that this model accounts very well for experimentally observed phase-resetting phenomenology (30). We use a variable time-step algorithm that is much more efficient than fixed time-step algorithms, yielding equivalent accuracy with much less computation (79). In addition, the convergence of the algorithm for equations of the Hodgkin-Huxley type used in this model can be mathematically proven (79). By adjusting the integration time step Δt at any time t to be 1 of the 10 values $2^N(0.016)$ ms with $0 \leq N \leq 9$, the change in the transmembrane potential ΔV in iterating from time t to time $t + \Delta t$ can be kept <0.4 mV in the simulations shown below (with one exception, see Fig. 15). When ΔV is >0.4 mV, the time step is successively halved and the calculation redone until a value of ΔV of <0.4 mV is achieved. When ΔV is <0.2 mV, the time step is doubled for the following iteration. In advancing from time t to time $t + \Delta t$, the current is calculated using the formula appearing in footnote 2 of Ref. 79. The time step is adjusted to a nonstandard value [i.e., $\neq 2^N(0.016$ ms)] when a current pulse is injected so that the pulse is turned on and off at exactly the right times. L'Hôpital's rule is applied when necessary in calculating the rate constants α_m, α_f, β_p, α_q, and β_q as well as the leakage current I_l. Initial conditions on V and the activation and inactivation variables are $V = -60.000$ mV, $m = 0.064260$, $h = 0.92720$, $d = 0.030477$, $f = 0.86991$, $p = 0.20890$, and $q = 0.012767$; the initial value of Δt is 4.096 ms. These initial conditions approximate, to five significant decimal places, a point on the cycle corresponding to spontaneous beating so as to minimize transients due to initial conditions. Calculations were carried out using programs written in FORTRAN on DEC VAX 750 and Hewlett-Packard 1000F minicomputers.

Bifurcation analysis. We used the computer program AUTO (21) to find equilibrium points and periodic orbits in the Irisawa-Noma equations and to evaluate their stability by calculation of eigenvalues and Floquet multipliers, respectively. This program generates bifurcation diagrams in which a solution branch corresponding to a particular equilibrium point or periodic orbit is followed ("continued") as a parameter is changed. A good introduction to eigenvalues, Floquet multipliers, and continuation techniques can be found in a recent textbook (71). We also briefly introduce each of these concepts as they make their appearance in RESULTS.

The double-precision version of AUTO (~16 significant decimal figures) was used throughout, with all calculations being carried out on a VAXstation 3100 or a DECstation 2100. The adaptable mesh option was used (IAD = 1), and derivatives were obtained numerically by differencing rather than being supplied analytically (JAC = 0). On the advice of Dr. A. Vinet, the number of mesh intervals (NTST) was increased from the default value of 10 to 250 and was of course doubled when period-doubled orbits were continued. The majority of other parameters in AUTO were left at their default values, including EPSL = 10^{-4}, EPSS = 10^{-4}, EPSU = 10^{-4}, ITMX = 8, ITNW = 5, MXBF = 5, NCOL = 4, NWTN = 3, THETAU = 0.0, THETAL (1) = 1. Other parameters (e.g., IRS, DSMIN, DSMAX, NMX) were altered depending on the characteristics of the particular solution branch being traced.

RESULTS

Spontaneous activity. Figure 1*A* shows spontaneous activity in the Irisawa-Noma model: V, the total transmembrane current (I_{tot}), and the individual ionic currents mentioned earlier are shown. The interbeat interval is 329.2 ms, the maximum diastolic potential is −65.8 mV, and the overshoot potential is 18.3 mV. These values are close to those appearing in the original description of the model (36). When double-precision arithmetic is used instead of single precision (16 vs. 7 significant decimal digits), we obtain traces that superimpose with those shown in Fig. 1*A*. In addition, decreasing the limits of the ranges of ΔV and Δt allowed by a factor of 10 using single-precision arithmetic produces very little change in the waveform, with, for example, the spontaneous interbeat interval increasing by <1%. In what follows, we have therefore used single-precision computation, the ΔV limits of 0.2 and 0.4 mV, and the Δt range 0.016 ms $\leq \Delta t \leq$ 8.192 ms.

During diastolic depolarization the changes in I_s and I_l in Fig. 1 are of comparable magnitude but are oppo-

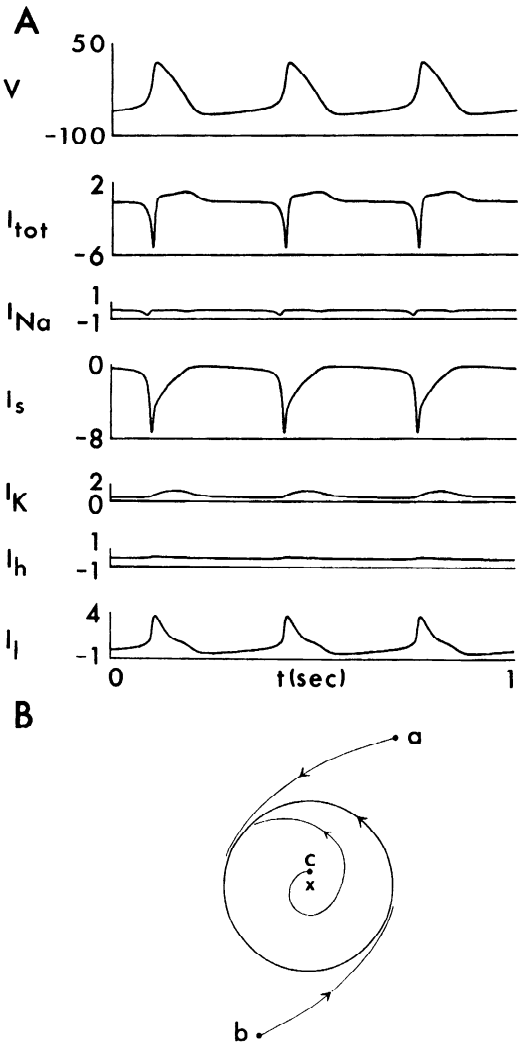

Fig. 1. Spontaneous activity in Irisawa-Noma model. *A*: transmembrane potential (V) and total transmembrane current (I_{tot}), fast inward sodium current (I_{Na}), slow inward calcium current (I_s), delayed rectifier potassium current (I_K), hyperpolarization-activated pacemaker current (I_h), and time-independent leakage current (I_l) as functions of time (t). Currents are all drawn to same scale and are expressed in units of μA/cm^2; V is in mV. Inward currents are negative in sign, outward currents are positive. *B*: simple 2-dimensional limit-cycle oscillator. Circle, (stable) limit cycle; x, (unstable) equilibrium point. Trajectories starting from 3 different initial conditions (*a*, *b*, *c*) are shown. Arrows indicate direction of movement along any particular trajectory as time progresses.

sitely directed. The changes in I_K, I_{Na}, and I_h are much smaller, with I_K changing considerably more than either I_{Na} or I_h. In fact, I_{Na} and I_h contribute little to the overall activity: removing them both from the model causes small changes in the waveform of the action potential and increases the spontaneous interbeat interval by ~20%.

In the Irisawa-Noma model, the state of the membrane at any given point in time is specified completely by the values of V, the activation variables m, d, p, and q (of I_{Na}, I_s, I_K, and I_h, respectively), and the inactivation variables h and f (of I_{Na} and I_s, respectively) at that point in time. These seven variables define a seven-dimensional state point (V, m, h, d, f, p, q) in the seven-dimensional state space of the system. Activity then corresponds to the movement of this state point in the state space, generating a curve called a trajectory. Starting out at time $t = 0$ from almost any initial condition (i.e., particular combination of V, m, h, d, f, p, q), the trajectory asymptotically (i.e., as $t \rightarrow \infty$) approaches a closed curve in the seven-dimensional state space. This closed curve is called a limit cycle or periodic orbit; the spontaneous periodic generation of action potentials shown in Fig. 1*A* (*top trace*) corresponds to the projection onto the V-axis of the periodic movement of the state point along this limit cycle. The limit cycle is said to be stable, since any trajectory starting out from an initial condition sufficiently close to the limit cycle is asymptotically attracted onto it. For example, injection of a current pulse produces a phase-resetting response in which recovery from the perturbation occurs as the trajectory asymptotically regains the limit cycle (30). In contrast, trajectories originating from initial conditions in the neighborhood of an unstable limit cycle would be repelled from the limit cycle.

The steady-state current-voltage (I-V) curve of the Irisawa-Noma model crosses the current axis at only one point, at $V \simeq -34.1266$ mV. Clamping the membrane to this potential therefore asymptotically results in zero current flow through the membrane. The other variables (i.e., m, h, d, f, p, q) approach the asymptotic values appropriate to that potential [e.g., $p \rightarrow p_\infty = \alpha_p(\alpha_p + \beta_p)^{-1}$, where α_p and β_p are the rate constants for p, the activation variable for I_K, evaluated at $V = -34.1266$ mV]. The set of initial conditions (V, m_∞, h_∞, d_∞, f_∞, p_∞, q_∞) for $V = -34.1266$ mV corresponds to an equilibrium point or steady state in the phase space of the system, since releasing the clamp should theoretically result in zero current flow and so quiescence. The fact that computationally the membrane does not rest at this equilibrium point when computations are started from initial conditions very close to it (see below) shows that this equilibrium point is unstable. Thus only if one were to start off at the exact set of initial conditions (specified to an infinite number of decimal places) and use infinitely precise computation would the membrane potential remain at $V \simeq -34.1266$ mV. There is also a set of initial conditions, apart from the equilibrium point, starting from any member of which the trajectory will asymptotically approach the equilibrium point. This set of points forms the stable manifold of the equilibrium point. When the equilibrium point is stable, the dimensionality of this set will be equal to the dimensionality of the system (7 in the case of the Irisawa-Noma model) so that starting out from any initial condition in a (perhaps relatively small) seven-dimensional neighborhood of the equilibrium point will result in a trajectory that is asymptotically attracted onto the equilibrium point. When the equilibrium point is unstable, the dimensionality of the stable manifold will be less than seven.

Because it is difficult to visualize dynamics occurring in a seven-dimensional state space, let us consider the simple schematic two-variable or two-dimensional limit-cycle oscillator shown in Fig. 1*B* to illustrate the above concepts. The closed curve is the limit cycle, with the arrow indicating the direction in which the state point moves along the cycle as time progresses. The limit cycle is stable, since starting from initial conditions, such as the points labeled *a*, *b*, or *c*, results in an asymptotic approach of the corresponding trajectory to the limit cycle. The equilibrium point is indicated by the symbol x and is unstable, since starting from an initial condition very close to the equilibrium point (e.g., *point c*) results in a repulsion of the trajectory away from the equilibrium point. Thus there are two structures of interest in the phase space of the two-variable system shown in Fig. 1*B* (and in the 7-dimensional phase space of the Irisawa-Noma model), an unstable equilibrium point and a stable limit cycle. Figure 1*B* (and other 2-dimensional sketches in Figs. 3, 4, 7, 8, 10, 12, and 15) is not to be regarded as a formal reduction of the full seven-dimensional state space of the Irisawa-Noma equations to a two-dimensional state space; instead it represents an intrinsically two-dimensional system used to illustrate concepts we introduce from nonlinear dynamics.

First way: gradual decline in action potential amplitude. In the first way of abolishing activity as some intervention takes hold, the action potential gradually and continuously decreases in amplitude until quiescence occurs. Figure 2 shows an example where the maximal conductance of I_s is decreased gradually in the model. Activity very similar in appearance can be seen in experiments in which I_s is progressively diminished using one of a variety of calcium-channel blocking agents (10, 40). In Fig. 2, the frequency of beating slowly decreases to about one-half of the initial frequency, and the amplitude of the action potential falls in a gradual smooth manner until spontaneous activity is extinguished, which agrees with the experimental result (e.g., see Refs. 10, 40). The first way is also seen experimentally in the SAN when many interventions other than blockade of I_s are carried out, e.g., application of Ba^{2+} (63) or injection of a constant depolarizing bias current (53, 55). In these two cases, analogous tracings can also be seen in the Irisawa-

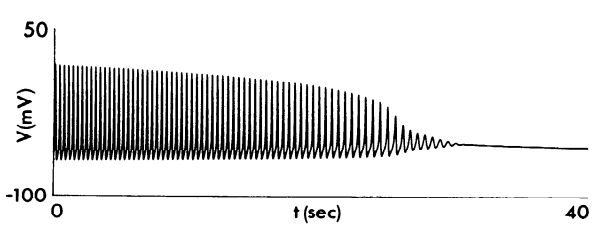

Fig. 2. V as a function of t as maximal conductance of I_s is gradually reduced to 0 in a linear fashion over 40 s.

Noma model when parameters appropriate to the particular experimental intervention are changed.

Figure 3 shows the behavior when the maximal conductance of I_s is reduced to increasingly smaller fixed levels and allowed to stay at each of those levels. At any given level of block in Fig. 3, *B–E*, spontaneous activity is seen, with the amplitude of the action potential as well as the frequency of beating declining as I_s is increasingly blocked. Finally, for the maximal conductance set to one-fifth of its normal value, spontaneous activity ceases (Fig. 3*F*).

During the normal spontaneous activity shown in Fig. 3*A*, an unstable equilibrium point and a stable limit cycle are present. As I_s is increasingly blocked (Fig. 3, *A–F*), the limit cycle contracts in size until it collapses onto the equilibrium point and disappears. Again, because it is difficult to visualize this in a seven-dimensional state space, Fig. 3, *G–I*, shows the analogous case in our simple two-dimensional limit-cycle oscillator. As a parameter is changed, the original limit cycle (Fig. 3*G*) shrinks in size (Fig. 3*H*), maintaining the same topology, i.e., a stable limit cycle and an unstable equilibrium point. Eventually, the limit cycle contracts down onto the equilibrium point and disappears (Fig. 3*I*), simultaneously converting the unstable equilibrium point in Fig. 3*H* into a stable equilibrium point in Fig. 3*I*. Thus at a value of the parameter somewhere between those used in Fig. 3, *H* and *I*, a bifurcation, a qualitative change in the dynamics, has occurred. The exact value of the bifurcation parameter (maximal conductance of I_s in the case of Fig. 3, *A–F*) at which the bifurcation occurs is termed the bifurcation value. The particular type of bifurcation occurring here in which the stability of an equilibrium point is reversed with the concurrent appearance or disappearance of a limit cycle is a Hopf bifurcation (1, 25, 71, 74).

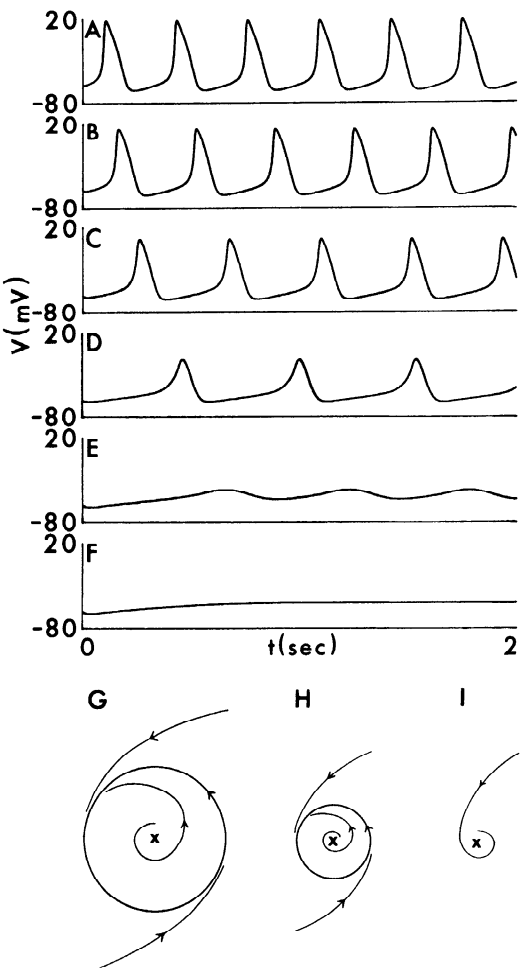

Fig. 3. *A–F*: Hopf bifurcation in ionic model. V as a function of t. Maximal conductance of I_s is reduced from its normal value (*A*) to 0.8 (*B*), 0.6 (*C*), 0.4 (*D*), 0.3 (*E*), and 0.2 (*F*) of that value. *G–I*: Hopf bifurcation in simple 2-dimensional system. As some parameter is changed, limit cycle (*G*) shrinks in size (*H*), eventually disappearing and reversing stability of equilibrium point (*I*). See text for further description.

Second way: annihilation. To the best of our knowledge, the second way of abolishing spontaneous activity in the SAN has been described only once, in experiments carried out on strips of kitten atrium containing nodal tissue placed in a sucrose gap apparatus (37). Injection of a subthreshold current pulse of the correct duration, amplitude, and timing could then abolish ("annihilate") spontaneous activity. Once activity was so annihilated, it could be restarted by injecting a second, suprathreshold current pulse. Although we know of only one report of annihilation in the SAN, the phenomenon has been described in several other cardiac preparations (20, 24, 38, 68, 72) and in other biological oscillators (35; see other refs. in Ref. 84).

These findings indicate the coexistence of two stable structures in the phase space of the system, a stable limit cycle and a stable equilibrium point, with the former corresponding to spontaneous activity and the latter to quiescence. In Hodgkin-Huxley-like systems, such as that studied here, it is relatively easy to locate equilibrium points. One simply plots the steady-state I-V curve and looks for zero-current crossings as described above. The voltage at which such a crossing occurs gives the V-coordinate of the equilibrium point, and the other coordinates (m, h, etc.) are obtained from the asymptotic values of those variables (i.e., m_∞, h_∞, etc.) appropriate to that potential. This procedure yields all equilibrium points present in the system, since $dV/dt = 0$ when the total current is zero for a space-clamped system, and the rates of change of all activation and inactivation variables are zero, since they are set to their asymptotic or steady-state values. The Irisawa-Noma model admits only one equilibrium point, since, as previously mentioned, there is only one zero-current crossing of its steady-state I-V curve (see Fig. 6 of Ref. 36). This equilibrium point is unstable, since starting computation from initial conditions very near to it results in a resumption of spontaneous activity (Fig. 4*A*). Thus annihilation cannot occur in the standard Irisawa-Noma model, since the only equilibrium point present is unstable. This prediction of the model agrees with the corresponding experimental finding in the rabbit SAN where clamping the membrane potential of a small, effectively isopotential piece of nodal tissue to the voltage corresponding to the zero-current point for some time and then releasing the clamp results not in quiescence but in the resumption of spontaneous beating (56).

However, the standard Irisawa-Noma model can be modified to allow annihilation. The first step in this process is to remove I_h. Removing I_h has only a small effect on the spontaneous frequency, as might be ex-

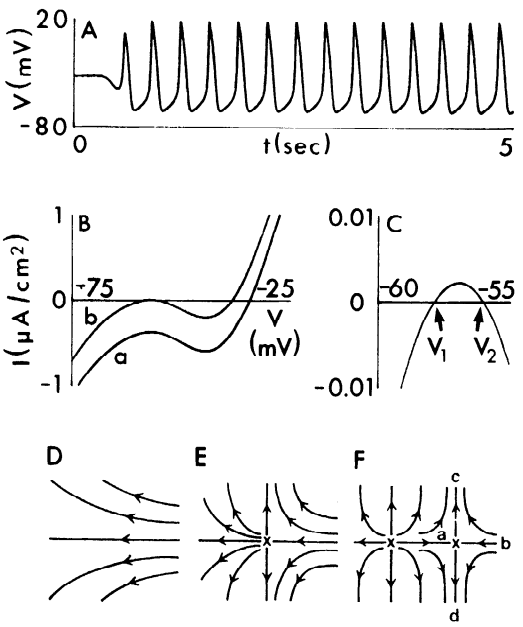

Fig. 4. *A–C*: saddle-node bifurcation in ionic model. *A*: integration is started from initial conditions appropriate to equilibrium point at $V = -34.1266$ mV in unmodified (i.e., $I_h \neq 0$) model. This simulation corresponds to clamping membrane potential for infinitely long time and then releasing clamp at $t = 0$. *B*: steady-state current-voltage (*I-V*) characteristic curve of model with I_h removed and bias current (I_{bias}) = 0.0 (*curve a*) or 0.392 $\mu A/cm^2$ (*curve b*). *C*: expanded view of *curve b* in *B* near equilibrium point at $V_1 \simeq -57.85$ mV with $I_{bias} = 0.392$ $\mu A/cm^2$. *D–F*: saddle-node bifurcation in 2-dimensional system. As some parameter is changed, a saddle-node equilibrium point (indicated by x) suddenly appears (*E*) in a region of phase space previously containing no equilibrium points (*D*). As parameter is changed further, saddle-node breaks up into 2 equilibrium points (*F*): an unstable node (*left*) and a saddle point (*right*).

pected from its small contribution to the total current during the phase of diastolic depolarization (Fig. 1*A*). This small contribution of I_h to generation of the pacemaker potential is seen in certain regions of the SAN, since blocking I_h pharmacologically sometimes produces only slight changes in the beat rate (12, 41, 57) and performing voltage-clamp experiments reveals that I_h is often present only in relatively small amounts (11, 12, 59). The *I-V* curve with I_h thus removed is shown in *curve a* of Fig. 4*B*. Note that because total current (*I*) is not a variable of the system, the *I-V* plane of Fig. 4*B* is not the state space, nor is it some projection of that space onto two dimensions. As in the unmodified model, there is only one zero-current crossing in *curve a* of Fig. 4*B*, showing that there is still only one equilibrium point in the model. Numerical simulation reveals that this equilibrium point is unstable, with a trace similar to that shown in Fig. 4*A*, which is from the unmodified model, being produced if one starts computation with initial conditions close to the equilibrium point. Injection of a constant hyperpolarizing bias current (I_{bias}) to slow further the spontaneous rate causes the *I-V* curve (*curve a*) of Fig. 4*B* to move upward. Eventually, because of the N-shape of the *I-V* curve, two new zero-current crossings of the *I-V* curve are created as the peak of the *I-V* curve moves through the voltage axis (*curve b* of Fig. 4*B*; expanded view in Fig. 4*C*), producing two new equilibrium points in the phase space of the system. There is thus, once again, a qualitative change in the dynamics, since two new equilibrium points (at potentials V_1 and V_2 in Fig. 4*C*) are created. This de novo creation of two new equilibrium points is called a saddle-node bifurcation of equilibrium points, with one of the points being a node and the other a saddle (1, 25, 74).

Figure 4, *D–F*, illustrates a saddle-node bifurcation in a two-dimensional system. Before the bifurcation takes place, there are no equilibrium points present in the part of the phase space shown in Fig. 4*D*, which also shows five representative trajectories. At the bifurcation point (Fig. 4*E*), there is the creation of a saddle-node, a special kind of equilibrium point. Note that this point exists at one and only one value of the bifurcation parameter, which is again called the bifurcation value. In Fig. 4*B*, the bifurcation parameter is I_{bias}, and the bifurcation value is the value of I_{bias} at which the peak of the N-shaped *I-V* curve just touches the *V*-axis at one point as I_{bias} is increased. At that exact value, a saddle-node equilibrium point is born via a saddle-node bifurcation. As the bifurcation parameter is pushed just beyond the bifurcation value (Fig. 4*F*), the saddle-node breaks up into two equilibrium points, one a saddle point (equilibrium point to the right in Fig. 4*F*) and the other a node (the equilibrium point to the left in Fig. 4*F*). The node is unstable in this case, since trajectories starting from anywhere very close to it leave its immediate vicinity. The saddle point is also unstable, since trajectories starting out from initial conditions almost anywhere in a small neighborhood around it leave its vicinity. However, there exist two sets of initial conditions that are attracted to the saddle asymptotically: starting off with an initial condition anywhere on the trajectories labeled *a* and *b* results in an asymptotic (i.e., as $t \rightarrow \infty$) approach to the saddle point. These two trajectories thus form the stable manifold of the equilibrium point, whereas the pair labeled *c* and *d* form the unstable manifold of the equilibrium point, since they asymptotically approach the equilibrium point should the direction of time be reversed. Each of these four trajectories (*a–d*) is termed a separatrix, since they separate the phase space in the neighborhood of the saddle point into four distinct regions. A trajectory cannot cross over from any one of these four regions into another. Thus a saddle point can confer on the membrane true all-or-none threshold behavior (17).

The equilibrium point created in Fig. 4*B* for the *I-V* curve labeled *b* and associated with the more depolarized potential, labeled V_2 in the exploded view of Fig. 4*C*, is a saddle; the other newly created equilibrium point, a node, is associated with the more hyperpolarized potential, labeled V_1 in Fig. 4*C*. A saddle point, as mentioned above, is always unstable. However, a node can be stable or unstable. Indeed, on being born at the bifurcation point, the equilibrium point associated with the potential V_1 is unstable. Thus annihilation is once again impossible. However, as I_{bias} is increased, there comes a point (at $I_{bias} \simeq 0.391$ $\mu A/cm^2$) where this equilibrium point reverses its stability: for example, by the point where the higher value of I_{bias} employed in Fig. 4*C* is reached, this equilibrium point has indeed become stable. Thus starting integration from an initial condition appropriate to that point results in quiescence (Fig. 5*A*, *trace a*); in contrast, if one starts from, for example, our standard initial condition (see METHODS), one obtains spontaneous activity (Fig. 5*A*, *trace b*). In this situation, activity can

therefore be triggered (Fig. 5*B*) or annihilated (Fig. 5*C*) by injecting a single current pulse. To trigger activity, the pulse must be large enough in amplitude; otherwise, only a damped subthreshold response, similar to that seen following annihilation in Fig. 5*C*, occurs. To annihilate activity, the current pulse amplitude, duration, and timing must all lie within certain critical ranges for a given polarity of the pulse. For the pulse polarity, amplitude, and duration used in Fig. 5*C*, annihilation is seen over a range of coupling intervals that is ~60 ms wide.

We have not been able to find annihilation in the standard unmodified (i.e., I_h not set to zero) model when I_{bias} is applied and changed in increments of 0.001 $\mu A/cm^2$, despite the fact that there is also in that case a range of I_{bias} over which three equilibrium points exist.

The equilibrium point with $V = V_1$ in Fig. 4*C* is stable, since starting out with an initial condition appropriate to that point results in quiescence (Fig. 5*A*, *trace a*). In this case, the system is six-dimensional, since I_h and its associated activation variable q have been removed. There is thus a full six-dimensional null space (6) surrounding the equilibrium point such that trajectories starting at an initial condition anywhere within this six-dimensional volume, which forms part of the stable manifold of the equilibrium point (the set of all initial conditions from which trajectories asymptotically approach the equilibrium point), are asymptotically attracted to the stable equilibrium point. Because periodic action potential generation can also be seen (Fig. 5*A*, *trace b*), a stable limit cycle producing that activity must also be present in the phase space of the system. Thus in the phase space of the system of Fig. 5*A* there are present at least four objects of topological interest: three equilibrium points, only one of which is stable, and one stable limit cycle. Because there is a full six-dimensional null space, there must be a five-dimensional surface (the separatrix surface) that divides the phase space into two regions. The presence of such a repelling hypersurface is necessary to produce a separation of trajectories, with trajectories starting from the set of initial conditions to the "inside" of the separatrix hypersurface, within the null space (which forms part of the basin of attraction of the equilibrium point) ending up at the equilibrium point, whereas those originating from most initial conditions outside the separatrix surface enclosing the null space (the basin of attraction of the limit cycle) asymptotically approach the stable limit cycle. Lying within this surface is an unstable limit cycle. How did this unstable limit cycle originate? We mentioned that the node created at the saddle-node bifurcation was unstable when born (at $I_{bias} \simeq 0.390$ $\mu A/cm^2$), but yet this equilibrium point was stable at the slightly higher value of I_{bias} (0.392 $\mu A/cm^2$) used in Fig. 5. Thus somewhere between $I_{bias} = 0.390$ and 0.392 $\mu A/cm^2$, there is a qualitative change in the dynamics that came about via a bifurcation, with the unstable equilibrium point reversing its stability, thereby becoming stable, and simultaneously spawning an unstable limit cycle in its immediate vicinity. The bifurcation is thus again a Hopf bifurcation. However, unlike the Hopf bifurcation shown earlier in Fig. 3, *G–I*, which is termed supercritical, since stable objects exist on both sides of the bifurcation, an unstable limit cycle is born rather than a stable limit cycle dying, which is termed a subcritical Hopf bifurcation, since unstable objects exist on both sides of the bifurcation. However, in both cases, the unstable equilibrium point becomes stable as the bifurcation parameter is changed.

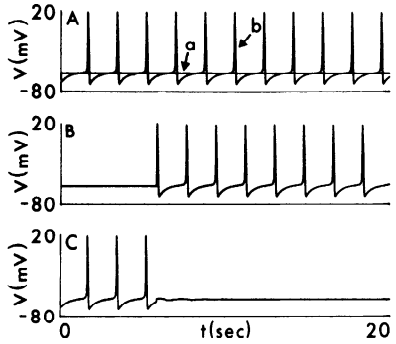

Fig. 5. Annihilation and single-pulse triggering in ionic model. *A*: $I_h = 0$ and $I_{bias} = 0.392$ $\mu A/cm^2$: integration is started from initial conditions appropriate to equilibrium point associated with potential V_1 in Fig. 4*C* in *trace a* and from our standard initial conditions (see METHODS) in *trace b*. *B*: injection of depolarizing current pulse (duration = 20 ms, amplitude = −2.0 $\mu A/cm^2$) at $t = 5.85$ s triggers activity (initial conditions corresponding to point V_1). *C*: injection of depolarizing current pulse (duration = 20 ms, amplitude = −0.2 $\mu A/cm^2$) at $t = 5.85$ s annihilates spontaneous activity (standard initial conditions).

The saddle-node and Hopf bifurcations described above are summarized nicely in a bifurcation diagram in which the value of one of the variables in a system is plotted as a function of the bifurcation parameter. In this case (Fig. 6*A*) we plot transmembrane potential vs. I_{bias}. The branch *abcde* of the bifurcation diagram of Fig. 6*A* is a plot of the voltage of the equilibrium point(s) as I_{bias} is changed. A solid curve indicates that the equilibrium point is stable, whereas a dashed curve indicates that it is unstable. As the hyperpolarizing bias current is increased, at *point d* in Fig. 6*A*, one has the saddle-node bifurcation depicted in Fig. 4*B* (*curve b*), when the peak of the N-shaped *I-V* curve intersects the voltage axis. At *point c* in Fig. 6*A* one has a reverse saddle-node bifurcation that results when the valley in the *I-V* curve of Fig. 4*B* is pushed up with further increase in I_{bias}, eventually intersecting the voltage axis and resulting in the coalescence and disappearance of two equilibrium points. Thus between the values of I_{bias} corresponding to the *points d* and *c* in Fig. 6*A*, the system has three equilibrium points, with the point lying along the branch *cd* being the saddle point with transmembrane potential V_2 in Fig. 4*C*.

Also shown on Fig. 6*A* are two curves *bf* and *bg*, which form the branch of the bifurcation diagram representing the stable periodic orbit responsible for the usual spontaneous generation of action potentials shown in Fig. 5, with *curve bf* giving the overshoot potential and *curve bg* giving the maximum diastolic potential at a particular value of I_{bias}. As with the gradual decrease of the conductance of I_s shown in Figs. 2 and 3, application of an increasingly large depolarizing bias current (i.e., moving from right to left in Fig. 6*A* from $I_{bias} = 0$) results in a gradual fall in the amplitude of this orbit, with both overshoot potential and maximum diastolic potential declining. Although we know of no corresponding systematic experiment with respect to injection of a depolarizing bias current, the partial experimental results now available (55) are consistent with this modeling

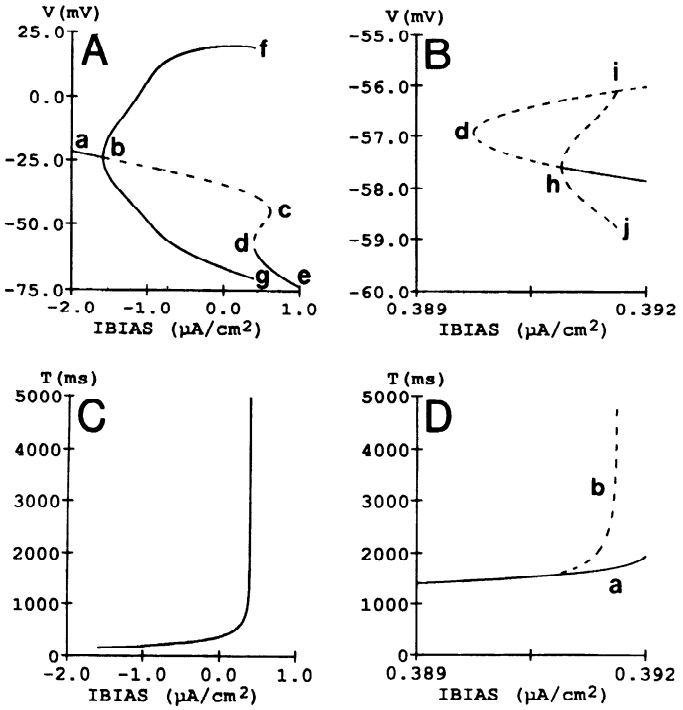

Fig. 6. Bifurcation diagrams generated with AUTO for ionic model with $I_h = 0$ (see text for further description). Exact values of I_{bias} at which phenomena (e.g., unstable limit cycle in *B*) occur are slightly shifted with respect to computations of Figs. 4 and 5, since double precision arithmetic and a different method of integration are used. *C*: period of stable limit cycle (*T*) is given as a function of the bifurcation parameter (I_{bias}). *D*: periods of both stable (*curve a*) and unstable (*curve b*) limit cycles are given; the 2 orbits approach homoclinicity within 0.0005 $\mu A/cm^2$ of each other (see also Refs. 16, 80).

result. At *point b*, a supercritical Hopf bifurcation occurs, with a stable limit cycle and unstable equilibrium point coalescing, being replaced by a stable equilibrium point (branch *ab*).

Figure 6*B* is an expanded view of Fig. 6*A* in a neighborhood of the saddle-node bifurcation (also termed knee, turning point, limit point, or fold) labeled *d* in Fig. 6*A*. The equilibrium point at the most negative potential in Fig. 6, *A* and *B* (V_1 in Fig. 4*C*), is unstable for I_{bias} sufficiently low (i.e., along *curve dh* in Fig. 6*B*) but is stable for higher I_{bias} (i.e., to the right of *point h*). This reversal of stability is caused by a subcritical Hopf bifurcation at *point h*, which produces a low-amplitude unstable limit cycle (*curves hi* and *hj* give the "overshoot" and maximum diastolic potentials of this orbit, respectively). There is thus only an extremely narrow range of I_{bias} (<0.001 $\mu A/cm^2$) over which the stable equilibrium point (branch to right of *h* in Fig. 6*B*) coexists with the small-amplitude unstable limit cycle of Fig. 6*B* (branch *hi-hj*) and the large-amplitude stable limit cycle of Fig. 6*A* (branch *bf-bg*), thereby allowing single-pulse triggering and annihilation to occur.

Once again, because it is difficult to exercise one's imagination in six dimensions, to illustrate the topological concepts underlying annihilation and single-pulse triggering we consider the simpler two-dimensional case shown in Fig. 7*A*. This is the simplest possible configuration in which it is possible to obtain annihilation and single-pulse triggering. Note that there is only one equilibrium point present (indicated by the x) that is stable, since starting from initial conditions sufficiently close to

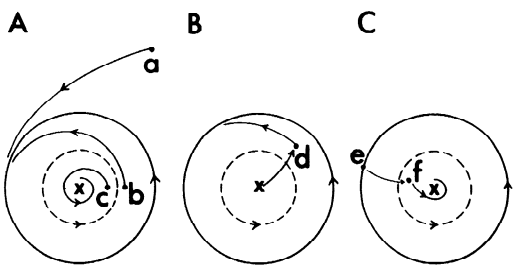

Fig. 7. Single-pulse triggering (*B*) and annihilation (*C*) in 2-dimensional system (*A*) possessing stable limit cycle (outer solid curve), unstable limit cycle (inner dashed curve), and stable equilibrium point (x). See text for further description.

that point (e.g., *point c*) results in an attraction of the trajectory asymptotically onto the equilibrium point. This point is analogous to the stable equilibrium point existing just to the right of *point h* in Fig. 6*B*. There are two limit cycles present, one lying inside the other. The outer limit cycle, the solid curve, is stable, since starting out at initial conditions at *points a* or *b* sufficiently close to it results in trajectories that asymptotically approach that limit cycle (Fig. 7*A*). Movement of the state point along this limit-cycle trajectory corresponds to spontaneous generation of action potentials in the Irisawa-Noma model (branch *bf-bg* in Fig. 6*A*). The inner closed dashed curve in Fig. 7*A* is an unstable limit cycle analogous to that existing in the Irisawa-Noma model (branch *hi-hj* in Fig. 6*B*). It is unstable, since trajectories starting out from initial conditions quite close to it (e.g., *points b* and *c*) are repelled away from it, eventually ending up at either one or the other of the two attracting structures in the phase space, the stable equilibrium point or the stable limit cycle.

Figure 7*B* illustrates the process of "single-pulse triggering" (Fig. 5*B*) in this configuration. Because the system is initially quiescent, this corresponds to the state point of the system sitting at the stable equilibrium point indicated by the x. In the absence of external perturbations, the state point will sit there indefinitely. Injection of a stimulus pulse can carry the state point away from the equilibrium point along the trajectory illustrated in Fig. 7*B*, with the state point ending up at *point d* at the end of the stimulus pulse. The trajectory will then wind out to the stable limit cycle as indicated. Thus spontaneous activity can be triggered by injecting a single stimulus pulse. It is apparent that the stimulus must be sufficiently large so that *point d* lies in the region exterior to the orbit of the unstable limit cycle; otherwise, the state point will return to the stable equilibrium point, following a trajectory similar to that shown in Fig. 7*A* starting from *point c*, giving a damped oscillatory subthreshold response, and triggering will not occur. In the case of Fig. 5*B*, the stimulus transports the state point through the five-dimensional separatrix hypersurface and thus out of the six-dimensional null space surrounding the equilibrium point.

Figure 7*C* illustrates an example of annihilation in the two-variable model. Starting during spontaneous activity, i.e., while the state point is moving along the outer limit cycle, which is stable, a stimulus is injected when the state point lies at *point e* on the stable limit cycle. The stimulus causes the state point to move along the trajectory indicated to *point f*, at which time the stimulus

pulse is turned off. The trajectory will then asymptotically approach the stable equilibrium point, which is attracting. Thus spontaneous activity is annihilated by injecting a single stimulus. In the case of annihilation shown in Fig. 5*C*, the stimulus again takes the state point to a point lying within the interior of the six-dimensional null space surrounding the equilibrium point, after piercing the separatrix hypersurface. It is apparent from the construction shown in Fig. 7*C* that only stimuli with certain combinations of strength and timing will leave the state point within the two-dimensional null space forming the interior of the unstable limit cycle. For example, a stimulus with the same timing as shown in Fig. 7*C*, but too small or too large in amplitude, might put the state point into the annular region lying between the two limit cycles (e.g., too large a stimulus delivered at *point e* might take the state point to *point b* in Fig. 7*A*) or even into the region outside the stable limit cycle. In both cases, one would have an eventual restoration of spontaneous activity due to asymptotic return of the state point to the outer, stable limit cycle. The region in the (stimulus strength)-(stimulus timing) parameter space at which annihilation will be seen has been termed the "black hole" by Winfree (84). In general, as the size of the unstable cycle grows (e.g., with increasing I_{bias} in Fig. 6*B*), one expects the size of this black hole to also grow.

The area within the interior of the unstable limit cycle in Fig. 7 is thus the stable manifold of the equilibrium point, since any initial condition within this area is attracted asymptotically onto the equilibrium point. In this simple two-dimensional system, the unstable limit cycle itself, which is a one-dimensional object, forms the separatrix in the system, since trajectories starting at initial conditions just to one side (inside) of this cycle asymptotically approach the equilibrium point, whereas those starting from initial conditions just to the other side (i.e., outside) go to the stable limit cycle. In contrast, in systems of dimension greater than two, the unstable cycle, being a one-dimensional object, cannot itself function as a separatrix but is embedded in the higher dimensional separatrix hypersurface.

The stable and unstable limit cycles shown in Fig. 6, *A* and *B*, are both born in Hopf bifurcations (at *points b* and *h*, respectively). They both gradually increase in amplitude (branch *bf-bg* in Fig. 6*A*, branch *hi-hj* in Fig. 6*B*) and then abruptly disappear. Just before disappearing, there is a very steep growth in the period of both oscillations (Fig. 6, *C* and *D*). The bifurcation producing destruction of both of these cycles is thus a homoclinic bifurcation (74) in which a periodic orbit collides with a saddle point and disappears.

Once again, it is easier to visualize this bifurcation in a simple schematic two-dimensional system (Fig. 8). We illustrate the homoclinic bifurcation analogous to that involved in abolishing the small-amplitude unstable orbit of Fig. 6*B* (branch *hi-hj*). One starts off with the situation in Fig. 8*A* where there is an unstable small-amplitude limit cycle (dashed curve) around a stable equilibrium point (*point a*), analogous to the point associated with V_1 in Fig. 4*C* (and located on the branch to the right of *point h* in Fig. 6*B*). There is also a saddle point (*point b*) analogous to the saddle point associated with V_2 in

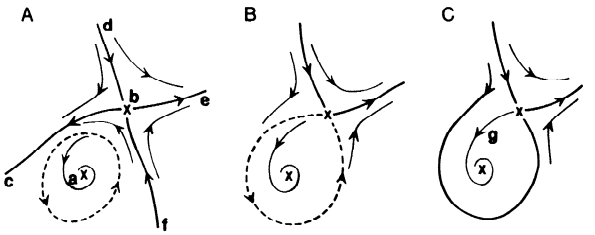

Fig. 8. Homoclinic bifurcation in simple 2-dimensional model. As bifurcation parameter is changed, unstable limit cycle initially present (dashed curve in *A*) grows in amplitude until it collides with saddle point (*point b* in *A*), producing a homoclinic orbit (dashed curve in *B*). As parameter is changed further, homoclinic orbit disappears, leaving a heteroclinic connection (trajectory labeled *g*) between saddle point and stable focus (*point a* in *A*). Reversing direction of all arrows on trajectories produces a homoclinic bifurcation in which a stable limit cycle is destroyed.

Fig. 4*C* (and branch *cd* in Fig. 6*A*). As the bifurcation parameter is changed, the unstable limit cycle of Fig. 8*A* grows in amplitude, with the state point increasingly slowing its rate of progress along the part of the orbit in the immediate vicinity of the saddle point. In fact, the period of the orbit becomes arbitrarily large as the saddle point, where by definition rates of change of all variables in the system are zero, is increasingly encroached on by the orbit. Eventually, at one exact value of the bifurcation parameter (the bifurcation value), the orbit collides with the saddle point and becomes of infinite period (Fig. 8*B*). At this point, one has an intersection of the stable and unstable manifolds of the saddle point, with the separatrix *bc* (Fig. 8*A*), which forms part of the unstable manifold of the saddle point, uniting with the separatrix *bf*, which forms part of the stable manifold of that point, to produce a single trajectory that is biasymptotic (i.e., as $t \rightarrow \pm\infty$) to the saddle point. This trajectory of infinite period is called a homoclinic orbit. Pushing the bifurcation parameter further (Fig. 8*C*) results in the disappearance of the homoclinic orbit into the blue, hence one alternative name for this bifurcation, the blue-sky catastrophe (74). The trajectory labeled *g* connecting the saddle point to the stable equilibrium point in Fig. 8*C* is termed a heteroclinic connection or orbit.

Even though we have chosen to illustrate the disappearance of a small-amplitude unstable limit cycle in Fig. 8, a similar scenario holds for the disappearance of the large-amplitude stable limit cycle at *point f-g* in Fig. 6*A*. In fact, the approach to homoclinicity of this orbit is heralded by the slowing in beat rate caused by the dramatic fall in the rate of diastolic depolarization seen in Fig. 5. This decrease is generated by the slow movement of the trajectory into a neighborhood of the saddle point, with subsequent rapid escape generating the upstroke of the action potential. The large-amplitude orbit characteristic of periodic action potential generation (branch *bf-bg*) thus disappears at large amplitude when hyperpolarizing I_{bias} is applied (at *point f-g*); in contrast, injection of depolarizing I_{bias} produces a gradual smooth decline in the amplitude of the action potential to zero (at *point b*).

Third way: skipped-beat runs. Figure 9 shows an example of the third way of abolishing spontaneous activity. A hyperpolarizing current is again injected to slow the rate of spontaneous activity but this time in the

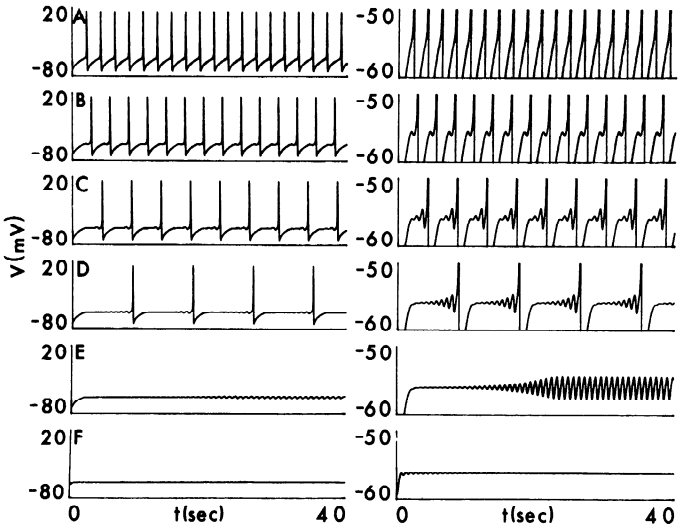

Fig. 9. Skipped-beat runs and subthreshold oscillation in ionic model. Spontaneous activity at 6 different values of I_{bias} in unmodified (i.e., $I_h \neq 0$) model: $I_{bias} = 0.78$ (A), 0.79 (B), 0.80 (C), 0.81 (D), 0.814 (E), and 0.818 (F) $\mu A/cm^2$. *Right*: range of potentials from −60 to −50 mV on expanded scale. Note appearance of prepotentials in B–D, a maintained small-amplitude oscillation in E, and a damped oscillation followed by quiescence in F. Standard initial conditions except for F where initial conditions corresponding to asymptotic values appropriate to $V = -55$ mV are chosen so as to make damped oscillation more evident.

unmodified (i.e., $I_h \neq 0$) model. At first, one sees a gradual slowing in the frequency of action potential generation until the interbeat interval grows to ~2 s (Fig. 9*A*). As I_{bias} is increased beyond this point, periodic patterns containing both action potentials and subthreshold incrementing oscillatory prepotentials ("skipped-beat runs") are observed. These prepotentials are more clearly seen in Fig. 9, *right*, which shows the pacemaker range of potential on an expanded scale. As I_{bias} increases, the frequency of occurrence of prepotentials relative to action potentials also increases (Fig. 9, *B–D*). Eventually a maintained subthreshold small-amplitude oscillation is seen (Fig. 9*E*). If I_{bias} is increased sufficiently, quiescence finally occurs (Fig. 9*F*). Patterns of activity very similar to various members of the sequence illustrated in Fig. 9 have been described in the SAN in response to a variety of interventions (e.g., see Refs. 9, 20, 39, 54, 55, 58, 62, 69, 76, 81). In the one instance of these reports in which it is straightforward to carry out the analogous simulation in the Irisawa-Noma model (adding acetylcholine), activity similar to that shown in Fig. 9 occurs in the model. Indeed, the entire sequence of patterns shown in Fig. 9 has been found in small pieces cut out of the SAN in which the external potassium concentration is gradually elevated and in the corresponding simulations on a modified version of the Noble-Noble (52) SAN model (M. R. Guevara, T. Opthof, and H. J. Jongsma, unpublished data). In that case, although excess K^+ causes a depolarization of maximum diastolic potential and not the slight hyperpolarization seen in Fig. 9, there is a progressive slowing in the rate of spontaneous diastolic depolarization similar to that shown in Fig. 9. This decrease in the rate of rise of the pacemaker potential is a common feature in many of the reports cited above in which skipped-beat runs have been described in the SAN; it is also seen in the Irisawa-Noma model and other SAN models when skipped-beat runs are produced by a variety of interventions (Guevara, unpublished data).

We now explore the bifurcation structure of the various rhythms of Fig. 9. We stress that these rhythms are only a sampling of those seen with I_{bias} between 0.780 and 0.818 $\mu A/cm^2$. For theoretical reasons outlined below, one expects an infinity of different rhythms, both periodic and aperiodic, to exist within this range. The rhythm shown in Fig. 9*D*, which is periodic with a very long period (10 s), suggests that the system is close to possessing a homoclinic orbit. This particular homoclinic orbit is not the same as that described earlier in Fig. 8 in that it is associated not with a saddle point but with a saddle focus. Once again, it is difficult to visualize trajectories in a seven-dimensional system: we therefore schematically illustrate in Fig. 10 a saddle-focus equilibrium point (indicated by the x) and its associated homoclinic orbit, which is the projection of an orbit in an inherently three-dimensional system down onto the two dimensions of a sheet of paper. Starting from an initial condition at *a*, which is a point on the homoclinic orbit close to the saddle focus, the trajectory first spirals outwards roughly in the plane of the paper and then makes an excursion out of that plane into the third dimension perpendicular to the plane of the paper (part of the trajectory labeled *b*). The orbit then reverses direction at *c*, returning toward the plane of the paper (part of trajectory labeled *d*). The speed of movement of the state point then slows, with the trajectory asymptotically (i.e., as $t \rightarrow \infty$) approaching the equilibrium point. Unlike the homoclinic orbit earlier illustrated in Fig. 8*B*, which involved a saddle point, the type of homoclinic orbit occurring in Figs. 9 and 10 cannot occur in a two-variable system. It requires a system of dimensionality of at least three, since, should the trace shown in Fig. 10 be regarded as being produced by a two-dimensional system, the trajectory would cross itself, thus violating uniqueness of solution.

Starting with an initial condition closer to the equilibrium point than the *point a* illustrated in Fig. 10 would result in the trajectory making a larger number of spiral turns in the plane before being ejected out into the third dimension. Starting with an initial condition infinitesimally close to the equilibrium point, an arbitrarily large

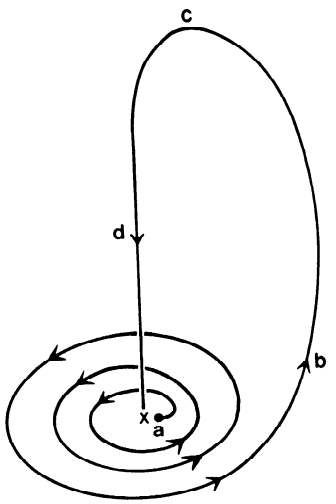

Fig. 10. Homoclinic orbit in 3-dimensional system. x, Equilibrium point, which is a saddle focus. See text for further description.

number of spiral turns of the trajectory would be produced, which would take an arbitrarily long time. A homoclinic orbit is thus a closed trajectory of infinitely long period, with the equilibrium point being both the starting and ending point of that orbit. Thus one would see, in terms of membrane potential, an infinite number of continually incrementing prepotentials (corresponding to the spiraling out in Fig. 10) that would take an infinitely long time to produce a single action potential, following which the membrane would asymptotically and monotonically return to its resting potential (corresponding to the approach to the saddle-focus point by the part of the trajectory labeled *d* in Fig. 10). Thus the simulations of Fig. 9 suggest that a homoclinic orbit involving a saddle focus likely exists at one precise value of I_{bias} somewhere between $I_{bias} = 0.810\ \mu A/cm^2$ (Fig. 9D) and $I_{bias} = 0.814\ \mu A/cm^2$ (Fig. 9*E*).

As I_{bias} is decreased away from the one exact value at which the homoclinic orbit involving the saddle focus exists, the homoclinic orbit disappears and one of two scenarios generally then occurs (23, 26, 82). In the simpler alternative, which unfortunately does not occur here, as the homoclinic orbit is broken one sees a single periodic orbit of finite period, with the period of that orbit smoothly decreasing as one moves the bifurcation parameter away from the bifurcation value at which the homoclinic orbit existed (e.g., see Fig. 3.1(i) in Ref. 26). The homoclinic orbit can then be regarded as the limiting case of this unique orbit as the bifurcation parameter is changed in the other direction back to the value producing homoclinicity. In the alternative, more complex, case that occurs here, more than one periodic orbit is born as the bifurcation parameter is moved through a range of values close to the value producing the homoclinic orbit of Fig. 10. The number of such orbits can be finite (e.g., see Figs. 3.8, 4.7 of Ref. 26) or infinite (e.g., see Fig. 3 of Ref. 23, Fig. 3.4 of Ref. 26, Fig. 3.2.41 of Ref. 82). In the simulations of Fig. 9, a large number of stable periodic rhythms are produced over a rather small range of I_{bias} ($\sim 0.03\ \mu A/cm^2$) adjacent to the value of I_{bias} at which the homoclinic orbit exists. In Fig. 9, we show only a few of these traces; however, many other more complex periodic rhythms (not shown) are seen when I_{bias} is changed more finely within the range $0.780\ \mu A/cm^2 < I_{bias} < 0.814\ \mu A/cm^2$.

How are these periodic orbits born, and how do they die? Some of these orbits are born through saddle-node bifurcations of periodic orbits, whereas others are born via period-doubling bifurcations (23, 26, 82). Figure 11, a partial bifurcation diagram computed using AUTO for the simulations of Fig. 9, gives examples of both of these bifurcations. As is the case when I_h is removed from the model (Fig. 6*A*), injection of a depolarizing bias current produces a supercritical Hopf bifurcation at *point b* (Fig. 11*A*), and there is again a region of coexistence of three equilibrium points in response to a hyperpolarizing bias current (Fig. 11*B*). However, there is not a subcritical Hopf bifurcation producing a small-amplitude unstable limit cycle in this region of coexistence, as in Fig. 6*B*, but rather a supercritical Hopf bifurcation at *point c* (Fig. 11*B*), which lies outside of this region, producing the small-amplitude stable oscillation of Fig. 9*E*. Thus, as direct numerical integration has already shown (Fig. 4*A*),

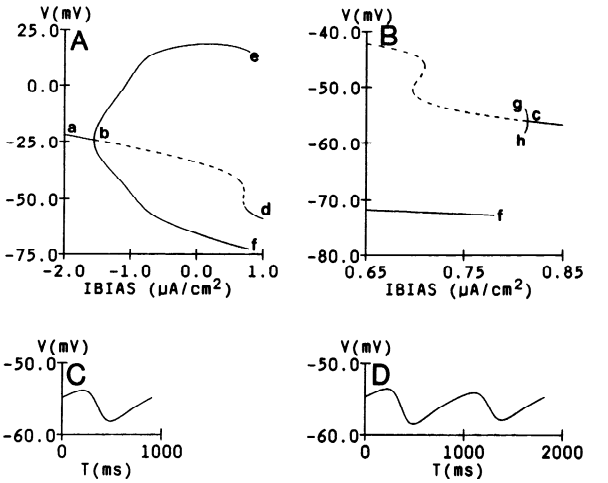

Fig. 11. *A* and *B*: bifurcation diagrams generated by AUTO in unmodified (i.e., $I_h \neq 0$) ionic model. *C*: stable small-amplitude subthreshold oscillation at value of I_{bias} ($\simeq 0.81102\ \mu A/cm^2$) close to maximum amplitude of orbit (*point g-h* in *B*). Slight decrease in I_{bias} results in a period-doubling bifurcation. *D*: stable period-doubled subthreshold oscillation at value of I_{bias} ($\simeq 0.81085\ \mu A/cm^2$) close to maximum amplitude. Further slight decrease in I_{bias} produces a second period-doubling bifurcation.

the annihilation and single-pulse triggering of Fig. 5 (I_h removed) cannot occur in the unmodified Irisawa-Noma model. Unlike the case in Fig. 6*B*, the small-amplitude orbit of Fig. 11*B* (branch *cg-ch*) does not terminate and vanish in a homoclinic orbit involving the saddle point, which is relatively far removed. Rather a period-doubling bifurcation occurs in which the small-amplitude limit cycle, stable along branch *cg-ch*, grows in amplitude as I_{bias} is decreased from its birth at *point c* until it becomes unstable at *point g-h*, spawning a stable limit cycle of about twice the period, but about the same amplitude, of the original but now destabilized limit cycle. This stable period-doubled orbit exists only over a very narrow range of I_{bias}, too small to be shown in Fig. 11*B*. It grows in amplitude as I_{bias} is reduced and itself undergoes another period-doubling bifurcation. Figure 11*C* shows one cycle of the small-amplitude oscillation at a value of I_{bias} just before it undergoes the first period doubling at *point g-h*, whereas Fig. 11*D* shows one cycle of the period-doubled oscillation just before it period doubles the second time. We return to discussion of period-doubled orbits at a later stage.

How does the large-amplitude limit cycle represented by branch *be-bf* in Fig. 11*A*, corresponding to the spontaneous action potential generation of Fig. 9*A*, disappear at *point e-f*? Again, the situation is different from that shown in Fig. 6*C* ($I_h = 0$): the limit cycle does not disappear abruptly in a homoclinic bifurcation as in Fig. 6*C*; rather, it collides with an unstable limit cycle and both orbits disappear at *point e-f* via a saddle-node bifurcation of periodic orbits. Although, for reasons previously mentioned, the traces shown in Fig. 9 can only be generated in a system having dimensionality of at least three, a saddle-node bifurcation of periodic orbits can occur in systems of dimensionality as low as two: Fig. 12 illustrates such a bifurcation in a simple two-dimensional system. In Fig. 12*A*, there are no periodic orbits present, only a stable equilibrium point. As the bifurcation parameter is changed, a large-amplitude limit

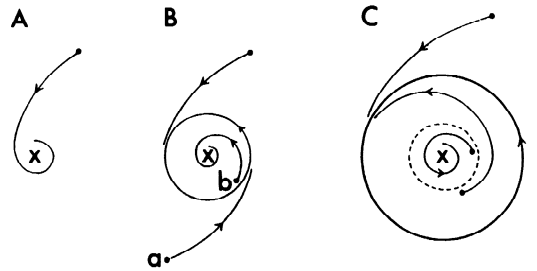

Fig. 12. Saddle-node bifurcation of periodic orbits in 2-dimensional system. As a parameter is changed to its bifurcation value, a large-amplitude semistable limit cycle (*B*) suddenly appears in a region of phase space previously containing no periodic orbits (*A*). As parameter is changed further, semistable cycle splits up into 2 limit cycles (*C*): one stable (outer solid curve) and other unstable (inner dashed curve). See text for further description.

cycle suddenly appears (Fig. 12*B*) via a saddle-node bifurcation of periodic orbits. The limit cycle is semistable, being attracting from one side (trajectory with initial condition *a* in Fig. 12*B*) but repelling from the other side (trajectory with initial condition *b*). Like the homoclinic orbits of Figs. 8*B* and 10, this semistable orbit exists only at one precise value of the bifurcation parameter, the bifurcation value (the value of I_{bias} corresponding to the *points e* and *f* in Fig. 11*A*). As the bifurcation parameter is pushed just beyond this point, the semistable limit cycle breaks up into two limit cycles, one stable and the other unstable (Fig. 12*C*). Note that the configuration shown in Fig. 12*C* is exactly that shown earlier in Fig. 7, which is the topology allowing annihilation and single-pulse triggering. Indeed, it is a saddle-node bifurcation generating stable and unstable limit cycles that allows these phenomena to occur in the Hodgkin-Huxley equations in response to injection of a steady bias current (see Fig. 9 of Ref. 35) instead of the homoclinic bifurcation of Fig. 6*B*.

Skipped-beat runs similar to some of those shown in Fig. 9 can be seen in the response of the model to I_{bias} if I_{Na} or both I_{Na} and I_h are removed. However, in the latter case these rhythms take place over a range of I_{bias} where there are three equilibrium points in the system. Because more than one equilibrium point is present, it is possible that heteroclinic connections, cycles, or orbits can occur, with trajectories connecting different equilibrium points (1, 71, 74, 82). In addition, because one of the three equilibrium points present is a saddle, it is possible that homoclinic orbits of the type illustrated in Fig. 8 exist about that point. The existence of hetero- and homoclinic trajectories can result in various bifurcations that produce or destroy limit cycles, e.g., the previously mentioned homoclinic bifurcation, as well as the omega explosion (74). This situation of coexistence of multiple equilibria when both I_{Na} and I_h are removed is in contrast to the unmodified model (Fig. 11, *A* and *B*), or when only I_{Na} is removed, or when I_l is increased in a reduced three-dimensional model (33) where skipped-beat rhythms occur when there is only one equilibrium point (a saddle focus) present in the phase space of the system. In addition, the basic rhythm of Fig. 9*A*, as well as at least some of the skipped-beat rhythms, can be annihilated and single-pulse triggered when both I_{Na} and I_h are removed, since the equilibrium point lying at the most hyperpolarized potential is stable in that circumstance (as in Fig. 4*C*).

Ionic mechanisms of skipped-beat runs. We now turn to investigate briefly the ionic mechanisms underlying the generation of the traces shown in Fig. 9. Figure 13 displays the various ionic currents during the rhythms shown in Fig. 9, *B* and *E*. Note that, as is the case during spontaneous activity (Fig. 1), the three currents I_{Na}, I_K, and I_h contribute but little to the evolution of the voltage waveform during diastole, and once again the changes in I_s and I_l are much larger, being almost exactly equal in magnitude but opposite in sign. The three indispensible currents involved in producing the skipped-beat rhythms shown in Fig. 9 can be said to be I_s, I_K, and I_l, since, if I_{Na} and I_h are both removed from the model, skipped beat runs can be seen at $I_{bias} \simeq 0.348\ \mu A/cm^2$. In addition, with I_{Na} and I_h both so removed from the model, which then becomes four-dimensional (variables: *V, d, f, p*), annihilation and single-pulse triggering can also be found. In fact, should the activation of I_s be made time independent (i.e., $d = d_\infty$ at all times), which is a reasonable approximation given the slow upstroke velocity of the action potential, the model becomes three-dimensional (variables: *V, f, p*) but is still capable of displaying annihilation and single-pulse triggering (33), as well as skipped-beat runs, both of which occur once again in a range of I_{bias} where there are three equilibrium points present in the system.

Afterpotentials and eigenvalues. In Fig. 9*F*, the membrane becomes quiescent in response to injection of a sufficiently large hyperpolarizing bias current. A decrementing oscillation of small amplitude is seen to precede the eventual establishment of quiescence in the steady state (Fig. 9*F, right*). If an action potential is provoked by a suprathreshold current pulse during this quiescence, one sees a train of decaying afterpotentials following the induced action potential that is similar to the damped oscillation shown in Fig. 9*F* but smaller in amplitude, indicating that the approach of the trajectory to the equilibrium point is modulated by currents activated

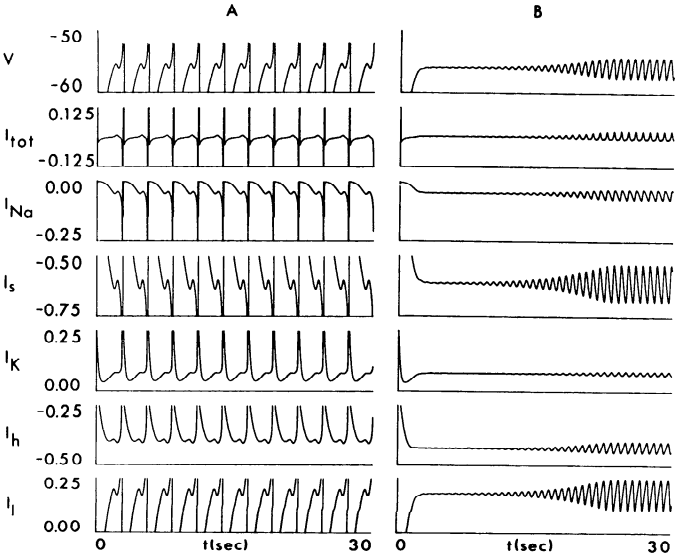

Fig. 13. Ionic basis of skipped-beat rhythm of Fig. 9*B* (*A*) and of subthreshold oscillation of Fig. 9*E* (*B*). Transmembrane potential and currents as in Fig. 1. All currents drawn to same scale.

during the action potential. Indeed, this behavior is seen as soon as I_{bias} is just large enough to produce quiescence. In that circumstance, injection of a subthreshold stimulus pulse produces a "ringing" in the membrane (Fig. 14*B*). As I_{bias} is increased, the damped oscillation starts off with a lower amplitude of its first peak and damps out more quickly (Fig. 14, *B–E*). Mathematically, the appearance of the damped oscillation as I_{bias} is increased is due to the conversion of the equilibrium point in the system of Fig. 14*A*, when a maintained subthreshold oscillation is present, from an unstable focus or spiral point to a stable focus via a Hopf bifurcation (at *point c* in Fig. 11*B*).

One can linearize the nonlinear Irisawa-Noma equations around the equilibrium point and calculate seven eigenvalues, numbers that characterize the behavior of the trajectories in an infinitesimally small neighborhood of state space about the equilibrium point (1, 2, 14, 25, 71, 74). When the oscillation in Fig. 14*A* exists, two of these eigenvalues are a pair of complex conjugate numbers with positive real part; the other five eigenvalues are negative real numbers. It is this positivity of the real part of the complex eigenvalue pair that makes the equilibrium point unstable and that is responsible for the trajectory spiraling away from it as time proceeds (Fig. 14*A*). As I_{bias} is increased, the real part of the complex pair decreases, and a Hopf bifurcation occurs, by definition, when the eigenvalues become purely imaginary, with zero real part (at *point c* in Fig. 11*B*). For I_{bias} greater than this bifurcation value, the real part of the pair of complex conjugate eigenvalues becomes negative, producing a stable equilibrium point (branch to right of *point c* in Fig. 11*B*). The fact that there is still a nonzero imaginary part of the eigenvalues results in oscillatory behavior, which is damped since the equilibrium point is stable (Fig. 14, *B–E*). As I_{bias} increases further, the real part of the complex pair becomes increasingly negative, leading to the progressively increasing level of damping shown in Fig. 14. In contrast, there is slower change in the imaginary part, leading to much smaller changes in the frequency of the damped oscillatory response. Eventually, at a sufficiently high value of I_{bias} (~1.17 $\mu A/cm^2$), the imaginary part of the complex pair of eigenvalues goes to zero, with the complex pair being replaced by two negative real eigenvalues, removing the oscillatory component of the dynamics but maintaining the stability of the equilibrium point. The stable focus is thus replaced by a stable node (1, 14, 25, 71, 74), with a monotonic (i.e., nonoscillatory) approach of the state point to the equilibrium point following a perturbation. A similar transition from a stable focus to a stable node occurs as an increasingly large depolarizing I_{bias} is injected at $I_{bias} \simeq -4.55$ $\mu A/cm^2$ (to the left of *point a* in Fig. 11*A*).

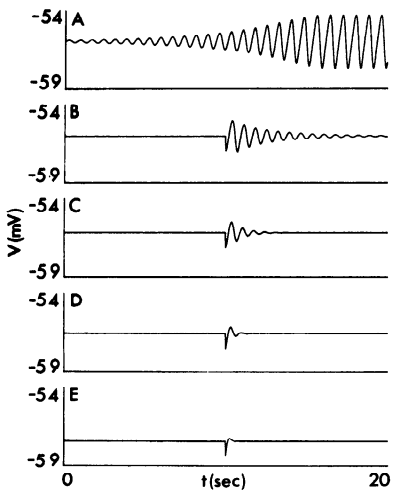

Fig. 14. Subthreshold potentials during quiescence. I_{bias} = 0.814 (*A*), 0.82 (*B*), 0.83 (*C*), 0.85 (*D*), and 0.90 (*E*) $\mu A/cm^2$. A maintained subthreshold oscillation is present in *A*. Membrane is quiescent in *B–E*, with a hyperpolarizing pulse of amplitude 0.05 $\mu A/cm^2$ and duration 20 ms injected at t = 10 s. Initial conditions in each case are close to equilibrium point, which is unstable in *A* but stable in *B–E*.

Limit cycles and Floquet multipliers. In the same way that one can linearize a system of nonlinear differential equations about an equilibrium point, one can also linearize a system about a limit cycle. Instead of obtaining eigenvalues, one obtains Floquet multipliers, which characterize the nature of the trajectories in an infinitesimal neighborhood of the limit cycle (71, 74). One of these multipliers is always equal to unity, reflecting the motion of the state point along the direction of the limit cycle trajectory itself. The other multipliers, which are $N - 1$ in number in an N-dimensional system, are generally complex numbers. The limit cycle is stable when all of those other $N - 1$ complex numbers lie within the unit circle. A stable limit cycle thus destabilizes through a bifurcation when one or two Floquet multipliers move away from the origin and eventually cross the unit circle as some parameter is changed. This can happen in one of three ways: a single real-valued Floquet multiplier crosses the unit circle by becoming more negative than −1, producing a period-doubling bifurcation; a single real-valued multiplier crosses through +1, producing a saddle-node bifurcation of periodic orbits; and a complex pair of multipliers intersects the unit circle, producing a torus bifurcation, after which orbits, which can be periodic or aperiodic, move on a toroidal hypersurface. In the first and third cases, the original limit cycle persists beyond the bifurcation point but is unstable. Thus it is numerical calculation of the Floquet multipliers using AUTO that allows us to determine the stability of the limit cycles in Figs. 6 and 11.

DISCUSSION

The traces presented above are not the first to show abolition of spontaneous activity in an SAN model as some intervention is made: for example, cessation of activity has been previously demonstrated as a result of adding a bias current (86), decreasing I_s (12, 75), adding acetylcholine (75, 86), increasing the internal sodium concentration (52), or blocking either of the calcium currents I_L or I_T (51). However, in these previous studies, the parameter under consideration was changed in steps too coarse to allow precise determination of how spontaneous activity would cease. In fact, the point of these other simulations was simply that spontaneous activity would disappear if the change made was sufficiently great. The present study is the first to probe finely the various routes leading to quiescence in an ionic model of SAN isopotential membrane.

First way. The first way of abolishing activity (Figs. 2

and 3) has been described as a result of several different interventions in the SAN (10, 40, 50, 63, 70). A common feature of these interventions is a gradual progressive primary reduction in either I_s or I_K, producing a continual smooth fall in the size of the upstroke or repolarization phase of the action potential, respectively. A fall in the size of either of these two phases also leads to a fall in the other: a primary decrease in I_s leads to a fall in overshoot potential, decreased activation of I_K, and a more depolarized maximum diastolic potential; a primary decrease in I_K produces a more depolarized maximum diastolic potential, increased resting inactivation of I_s during diastole, and a fall in the overshoot potential. Thus, in both cases, the action potential amplitude (the difference between overshoot and maximum diastolic potentials) declines. As in Figs. 2 and 3, where I_s is blocked, blocking I_K in the Irisawa-Noma model also produces a gradual fall in action potential amplitude.

Second way. Annihilation and single-pulse triggering become possible when there is coexistence of a stable equilibrium point and a stable limit cycle (Fig. 7). Indeed, it was this theoretical concept that led Appleton and van der Pol (4) in 1922 to search for and find single-pulse triggering in a simple electronic oscillator. Indeed, oscillators with the topology shown in Fig. 7*A* are referred to in the engineering literature as "hard" oscillators, since they must be excited in some way with a shock of finite amplitude to be started up (in contrast to the "soft" oscillator of Fig. 3*G*). Teorell (see Ref. 73 and references to earlier work contained therein) invoked the concept of a hard oscillator to explain the "single-pulse initiation" and "brief-pulse annihilation" that he had observed in analogue computer simulations of a physical model of a mechanoreceptor. It was also theoretical work, based on consideration of the topology of phase resetting and the implied existence of a "singular stimulus," that led Winfree (83) some years later to independently propose the concept of annihilation. This pioneering work of Winfree directly led experimentalists to conduct the first systematic searches for annihilation in several biological preparations, including cardiac tissue (35, 37, 38). Although several examples of a premature stimulus annihilating spontaneous activity had appeared in the cardiac literature before these systematic searches were made (see discussion in chapt. VIII of Ref. 20), no theoretical interpretation of those isolated results was offered.

Annihilation. Although there are many experimental studies showing at least some features of the first and third routes to quiescence in the SAN, we know of only one report in which this second route (annihilation) has been described in the SAN (37). As previously noted, the results of another experimental study indicate that annihilation should not be possible (56). The reasons for the diametrically opposing results in these two studies are unknown; they might, for example, simply involve species differences [cat (37) vs. rabbit (56)] or differences in the experimental preparation [sucrose-gap (37) vs. small piece (56)]. However, it must be kept in mind that the SAN is an inhomogeneous structure with, for example, action potentials of many different morphologies being recorded in different areas of the node (7). Thus the contrasting results of Jalife and Antzelevitch (37) and Noma and Irisawa (56) might be due to differences in the sites from which the SAN specimens were taken. Recent work has shown that many of the electrophysiological differences in small pieces of tissue taken from different sites are largely intrinsic, being local properties of the cell membrane, and are not due to electrotonic interactions (39, 41, 61). This conclusion is reinforced by more recent work using single SAN cells (59).

In some pieces of tissue isolated from the SAN, voltage-clamp experiments indicate that I_h is present only in relatively small amounts in the pacemaker range of potential, and so I_h would be expected to play a negligible role in generating spontaneous diastolic depolarization in those pieces (11, 12). More recent work on single cells isolated from electrophysiologically unidentified areas of the SAN indicates that there is significant variability in the amount of I_h (pA/pF) present in different cells (59). In fact, blocking I_h with Cs^{2+} in some small-piece preparations produces only a slight decrease in rate (12, 41, 57). In contast, in other pieces, a significant amount of I_h is activated by a voltage-clamp step into the pacemaker range of potentials (11, 12, 48), and relatively large changes in beat rate can be produced when Cs^{2+} is applied (12, 41, 57). In the Irisawa-Noma model in which a hyperpolarizing bias current is applied, our work indicates that I_h must be absent (or sufficiently reduced) for annihilation to be seen. The exact degree of reduction is very delicate, depending on the details of the model. For example, in the predecessor of the Irisawa-Noma model, which also has a small contribution of I_h, it is not necessary to reduce I_h to see annihilation (43). In this respect, it is interesting to note that in both experimental and modeling work on two other cardiac tissues in which annihilation has been demonstrated [depolarized Purkinje fibre (15, 38, 68), depolarized ventricular muscle (16, 24, 68)], one would also expect a negligible contribution of I_h to the generation of diastolic depolarization.

In addition, in all three of these tissues, I_{Na} is substantially reduced as a consequence of inactivation secondary to depolarization of the membrane, a feature shared with the Irisawa-Noma model. In a very recent report using a fourth preparation, the embryonic chick atrial heart cell aggregate, which does not possess I_h, annihilation could not be produced unless I_{Na}, which is relatively large in this preparation, was at least partially blocked with tetrodotoxin (72). Computer simulation using an ionic model of this preparation is also in agreement with this experimental finding (72). Once again, different areas of the SAN show evidence of intrinsically possessing radically different amounts of I_{Na} (39, 41, 61). Finally, in the one reported case of annihilation in the SAN, the interbeat interval was quite long for a kitten [~390 ms in Fig. 1 and ~670 ms in Fig. 2 of Ref. 37 vs. a mean interval of 375 ± 41.4 (SD) ms in 12 isolated SAN preparations from cats weighing 2.5–4.5 kg in Ref. 60]. This is consistent with our finding in the model (Fig. 5*C*) that annihilation is only seen when the interbeat interval is prolonged significantly by, for example, injecting a hyperpolarizing bias current. The fact that annihilation is not seen in the model with I_h present in sufficiently large amounts might indicate that I_h is playing a protective role in the peripheral areas of the SAN, where it is present in considerable amounts, in that it prevents annihilation from occurring in the primary natural pace-

maker of the mammalian heart in response to an otherwise suitably timed premature atrial contraction. The study with atrial aggregates mentioned above might also indicate that I_{Na} is playing a similar protective role in peripheral areas of the node where it is also present in large amounts.

One other point that might have some bearing on the differences in the two studies is the fact that the equilibrium point that is created anew (at voltage V_1 in Fig. 4*C*) as I_{bias} is changed can be stable, thus allowing annihilation to be seen. For this point to be created, the steady-state *I-V* characteristic curve must be N-shaped, having a region of negative slope. However, most published *I-V* curves from the SAN have an N-shaped region that is either very shallow or even entirely absent (48, 53, 57). Indeed, in the Irisawa-Noma model, either modified (by removing I_h) or unmodified, the *I-V* curve is very shallow, with the region of negative slope conductance disappearing if, for example, the I_{Na} window current is removed. Therefore three equilibria exist over only a very small range of the parameter being changed ($0.3897\ \mu A/cm^2 < I_{bias} < 0.6085\ \mu A/cm^2$ in the case of Fig. 6*A*), and the possibility of annihilation exists only over a much smaller part of this already small range ($0.3909\ \mu A/cm^2 < I_{bias} < 0.3916\ \mu A/cm^2$ in Fig. 6*B*). In Purkinje fiber and ventricular muscle, the N-shaped region of negative-slope conductance is much more prominent. Single-pulse triggering and annihilation resembling that shown in Fig. 5, i.e., with the resting potential lying in the pacemaker and not the plateau range of potentials, can be seen in a model of Purkinje fiber with I_h removed (Guevara, unpublished data) and in models of ventricular muscle (16, 80), which do not possess I_h, in response to injection of a depolarizing bias current. In both cases, the *I-V* curve has three zero-current crossings when these phenomena occur (Guevara, unpublished data and Refs. 16, 80, respectively). Because voltage-clamp studies were not carried out in the one reported case of annihilation (37), one cannot say at this time whether the existence of an N-shaped *I-V* curve is crucial in allowing annihilation to be seen in the SAN, as Figs. 4 and 5 might indicate. Nevertheless, in the one reported case of annihilation in the kitten SAN (Fig. 1 of Ref. 37), the membrane potential did come to rest at about −53 mV. This zero-current potential is ~15–20 mV hyperpolarized with respect to that in the rabbit SAN (56) but is consistent with the scenario in Fig. 4, *B* and *C*.

In all of the above, we have used the term annihilate to mean the permanent cessation of spontaneous action potential generation following injection of a brief-duration stimulus. By permanent, we mean that the membrane remains quiescent indefinitely in the absence of any subsequent externally applied stimulation. Thus we are not using the term to refer to a rather long, but temporary, arrest or pause of action potential generation, a sense in which the term annihilation has been used (65). Although such very long pauses, of the order of several cycle lengths, have been described in response to delivery of a current pulse in an ionic model of the SAN (65), we are not aware of any corresponding description in experimental work on the SAN. However, temporary pauses have been described experimentally in depolarized Purkinje fiber (38) and in aggregates of embryonic chick ventricular cells (17, 32), as well as in models of both of these tissues (17, 32). During such a pause, one often sees an incrementing small-amplitude oscillation (e.g., see Fig. 1*B2* of Ref. 38 and Fig. 5 of Ref. 32). Such behavior is expected if the state point of the system is perturbed into a neighborhood of the stable manifold of an unstable equilibrium point possessing a pair of complex conjugate eigenvalues with positive real parts. In modeling work, starting numerical integration from initial conditions close to the equilibrium point itself produces incrementing small-amplitude oscillatory activity (Fig. 4*A*; see also Fig. 9 of Ref. 31 for the case of Purkinje fiber). The corresponding experiment has been carried out in the SAN (see Fig. 8 of Ref. 56).

When the system admits a stable equilibrium point, only certain critical combinations of amplitude, duration, and timing ["portal" of entry (6)] for a given polarity (i.e., depolarizing or hyperpolarizing) stimulus will result in annihilation. This property was probably first remarked on in a biological context by Teorell (73), who noted that the pulse had to be placed "strategically," with the "vulnerable" region for a depolarizing stimulus coinciding with the refractory period. At a given polarity and pulse duration, the combination of stimulus amplitude and timing defines the black hole (15, 16, 84) in the two-dimensional (amplitude, timing) stimulation parameter space, with the size of the black hole depending on stimulus duration (73). At this point, we wish to repeat a cautionary note initially sounded by Teorell (73): inability to produce annihilation by executing phase-resetting runs over a wide range of stimulus amplitude at a given pulse duration is not conclusive proof that the equilibrium point is unstable, since the possibility exists that annihilation could occur at some other pulse duration. In such instances one can traverse the type 1-type 0 phase-resetting border by crossing a part of the stable manifold of the equilibrium point that is not a part of the full-dimensional null space, obtaining a direct transition from type 1 to type 0 phase resetting without producing annihilation. Thus, in instances where this direct transition is recorded experimentally (32, 78), there is no guarantee that a full-dimensional null space is not present, which might be accessible should some other pulse duration be used. However, in the former study (32), modeling work shows the equilibrium point to be unstable (17). Thus inability to produce annihilation in some fraction of preparations within a given study (e.g., see refs. in chapt. VIII of Ref. 20 and Refs. 37, 38, 72) might be at least partly due to inappropriate choice of pulse duration for a given preparation. Indeed there is no a priori reason to suppose that, should the equilibrium point be stable, there must be some physiological combination of stimulation parameters that would allow annihilation to be manifested. About the only unequivocal way to determine that annihilation is impossible is to find all equilibrium points by constructing an *I-V* curve and then to demonstrate that all these points are unstable by clamping the membrane to each of these voltages in turn, allowing sufficient time for transients to pass, releasing the voltage clamp, and seeing that spontaneous activity resumes (e.g., see Fig. 8 of Ref. 56).

Single-pulse triggering, triggered activity, and afterpotentials. The converse of annihilation, single-pulse trig-

gering (Fig. 5*B*), has been reported in SAN tissue made quiescent by reduction of the external sodium concentration (81), by overdrive suppression following partial blockade of I_s (19), by application of papaverine (69), or by annihilation itself (37). However, in the first study, spontaneous activity was only transiently reestablished, which was also sometimes the case in the second and third studies. Transient single-pulse triggered activity can also be seen in Purkinje fiber (19, 20). We stress here that single-pulse triggering of the sort shown in Fig. 5*B* is not identical with one form of activity commonly described as "triggered activity" in which it is necessary to apply a train of two or more stimuli during quiescence (18, 20), since a single suprathreshold stimulus is then not sufficient to trigger activity. Perhaps the simplest way to induce triggered activity is to apply two closely coupled suprathreshold stimuli and then progressively decrease the coupling interval. One then sees a gradual growth in the height of the delayed afterdepolarization following the second action potential as the coupling interval is reduced. Eventually, this afterpotential attains threshold, producing one or more nondriven action potentials, perhaps even a sustained rhythm. No such effect is seen in the Irisawa-Noma model. This is not surprising, given that this growth in the afterpotential size is attributed to the transient inward or oscillatory current (I_{ti} or I_{os}, respectively), which is not incorporated in this model. We are not aware of any unambiguous reports of triggered activity in the SAN; in reports in which a train of stimuli starts up activity (e.g., see Ref. 69), it is not clear that a single stimulus would not have had the same effect. We propose that the term single-pulse triggering be used to describe the form of triggering seen in Fig. 5*B* to discriminate this form of initiation of spontaneous activity from triggered activity.

Delayed afterdepolarizations following stimulation of an action potential during quiescence have been described in the SAN when the external Na^+ concentration is decreased (56, 81) or when papaverine is added (69) and in other areas of the heart in response to a wide variety of interventions (18, 20). These afterpotentials are usually attributed to the presence of I_{ti}, which has recently been described in voltage-clamp experiments on the SAN following exposure to a low-K^+ solution (13). However, it is possible to see delayed afterdepolarizations in the Irisawa-Noma model, as well as in a model of ventricular muscle (Guevara, unpublished data), neither of which includes this current. Afterdepolarizations occur in the model when the membrane is quiescent, but on the verge of becoming spontaneously active (Fig. 9*F*), when the equilibrium point possesses a pair of complex conjugate eigenvalues with negative real part. The existence of such eigenvalues produces a stable focus or spiral point, as described above, and therefore results in the damped oscillatory approach to the resting potential shown in Fig. 14, *B–E* (see Refs. 14, 47 for a detailed analysis of the analogous situation in squid giant axon). This finding suggests that in situations where I_{ti} is assumed to be implicated in generating triggered activity, it might very well be that afterpotentials seen before the onset of such activity stem, at least in part, from non-I_{ti} mechanisms similar to those shown in Fig. 13, *left*. In a similar vein, in the many circumstances in which one sees rhythms consisting of incrementing prepotentials intermixed with action potentials (20), the presence of I_{ti} might not be needed to account for these rhythms (e.g., Fig. 9).

Third way. In contrast to annihilation, there have been many reports in which skipped-beat runs similar in appearance to those shown in Fig. 9, *B–D*, have been described in sinus tissue. Interventions that produce skipped-beat runs include increasing the external K^+ concentration (9, 53, 56), decreasing the external Na^+ concentration (55, 81), decreasing catecholamine levels (76), adding papaverine (69) or acetylcholine (9, 39) to the bathing solution, blocking the Na^+-K^+ pump by reducing the extracellular K^+ concentration (54), and increasing the osmolarity of the bathing fluid (58). A common feature of all of these interventions is that there is a dramatic slowing in the rate of rise of the pacemaker potential. Skipped-beat runs can also be seen in simulations when changes corresponding to several of the above interventions are made in various SAN models (Guevara, unpublished data). Thus skipped-beat runs have been found in a variety of very different situations: in fact, our search of the literature leads us to conclude that the third way of abolishing spontaneous activity is the most pervasive of the three, which is perhaps unfortunate, since it is also the most complicated of the three.

Unlike skipped-beat runs, there are only rare experimental reports of a maintained small-amplitude oscillation in sinus tissue following a sequence of skipped-beat runs (9, 54). Figure 9*E* shows that a maintained subthreshold oscillation, and not quiescence, can indeed be regarded in some sense as a limiting case of skipped-beat runs of arbitrarily long period. The fact that the range of the control parameter (I_{bias} in this case) over which this oscillation is seen is very narrow might explain why it has been so rarely described in experimental work. In fact, in our own experimental and modeling work in which the external K^+ concentration is gradually raised, one must adjust the K^+ concentration exquisitely to obtain a maintained subthreshold oscillation (Guevara et al., unpublished data). A similar proviso holds in other experimental and modeling work in which the oscillation is seen in response to a variety of different interventions (Guevara, unpublished data).

The isolated observation of a small-amplitude oscillation is not enough to guarantee that the third route is being followed, since such an oscillation can also be seen in the first way (e.g., see Fig. 3*E*). In addition, one must not confuse the waveforms of Fig. 9, *B–E*, with those due to block of propagation, which produces well-separated electrotonic "bumps," often showing clearly defined rising and falling exponentially shaped phases superimposed on the resting potential or the pacemaker potential (10, 44, 64).

Chaotic dynamics and period-doubling bifurcations. Waveforms strikingly similar to those shown in Fig. 9 have been described in other biological, chemical, and electronic oscillators as well as in simplified low-dimensional models of such systems (see Refs. 5, 16, 20, 23, 26–28, 33, 46, 71, 82 and references therein). In many of these reports the existence of deterministically irregular or "chaotic" dynamics is claimed. As previously mentioned, the trace shown in Fig. 9*D* indicates that the

system is close to possessing a homoclinic orbit biasymptotic to a saddle-focus equilibrium point. It is now well known that the breakup of this kind of homoclinic orbit can produce chaotic dynamics, the Shil'nikov phenomenon (23, 26, 82). The condition on the real parts of the eigenvalues of the saddle focus at homoclinicity that are sufficient {but not necessary [see Fig. 4.9(ii) of Ref. 26 and associated description]} to guarantee the existence of Shil'nikov chaos, real part of complex conjugate pair less than absolute value of all other (real) eigenvalues, are indeed fulfilled in the system of Fig. 9. This chaotic dynamics arises via a cascade of period-doubling bifurcations (e.g., see Figs. 4.2 and 4.8 of Ref. 26). However, we have not observed period-doubling rhythms or irregular dynamics in our numerical integration of the Irisawa-Noma equations in single precision (Fig. 9) even when I_{bias} was changed in the sixth significant decimal place in regions where such behavior is to be expected (e.g., between the values of I_{bias} used in Fig. 9, *B* and *C* and *D* and *E*). This is not surprising, given that the range of the bifurcation parameter (I_{bias}) over which these behaviors are expected to occur is very narrow (e.g., see Fig. 4.8 of Ref. 26) and that the chaotic behavior in this form of chaos has a very small-scale or fine-grained nature, being apparent only if traces are examined at quite high magnification (see Fig. 6 of Ref. 5). However, we do have evidence in the double-precision calculations of Fig. 11 for two successive period-doubling bifurcations of the small-amplitude orbit of Fig. 9*E*. The first period-doubled orbit is stable over a range of I_{bias} of only $\sim$0.00017 $\mu A/cm^2$, and one expects any higher order period-doubled orbits to be stable over increasingly smaller intervals of I_{bias}. From the point of view of an experimentalist, the argument becomes largely academic, since it would be exceedingly unlikely that one could observe such rhythms in the corresponding experimental work due to the presence of membrane noise, which would especially corrupt the low-amplitude subthreshold activity (see Fig. 6*a* of Ref. 5). Indeed, we have only infrequently observed a transient rhythm similar to the period-doubled rhythm of Fig. 11*D* in our experiments involving change of external K^+ concentration. In one very careful experimental study on a chemical oscillator in which patterns similar to those shown in Fig. 9 were described, no trace of aperiodic dynamics could be found (46). A subsequent modeling study showed evidence of small-scale chaos over very narrow ranges of the bifurcation parameter; however, the chaos was judged to be on "a scale too small to be observable in laboratory experiments" (see Fig. 6 of Ref. 5). Further discussion about the possible existence of chaotic dynamics can be found in Ref. 33, where a simplified three-dimensional version of the Irisawa-Noma model is investigated, with rhythms similar to some of those shown in Fig. 9 being seen as I_1 is increased.

Although we have not observed period-doubling bifurcations in the single-precision numerical integrations of Fig. 9, as would be expected since Shil'nikov chaos exists (23, 26, 82), we have found a period-doubling bifurcation in the Irisawa-Noma model when the maximal conductance of I_s is increased (Fig. 15) instead of decreased as earlier in Figs. 2 and 3 (which produced a Hopf bifurcation). Note the beat-to-beat alternation in action potential parameters, most noticeably the maximum diastolic potential, in Fig. 15*B*. Alternation in action potential morphology has previously been described in the SAN at least once, in an experiment in which isoproterenol, which augments I_s, was applied (81). As is the case with a homoclinic orbit, a period-doubled orbit can exist only in a system with dimension greater than or equal to three, since in a two-dimensional system the period-doubled orbit would have to cross itself, thus violating uniqueness of solution. Figure 15*C* shows a projection of a limit cycle in such a high-dimensional system onto the plane of the paper. This limit cycle undergoes a period-doubling bifurcation producing a period-doubled orbit (solid curve in Fig. 15*D*). Note that the original orbit is still preserved but has become unstable (dashed curve in Fig. 15*D*), repelling nearby trajectories onto the stable period-doubled orbit.

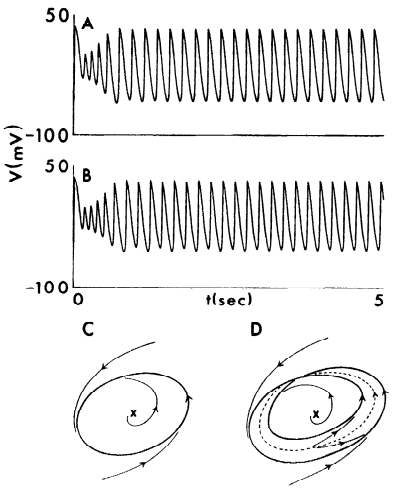

Fig. 15. *A* and *B*: period-doubling bifurcation in ionic model. Effect of increasing maximal conductance of I_s to 4.9 (*A*) and 5.0 (*B*) times its standard value. A period-doubling bifurcation occurs for maximal conductance somewhere between 4.9 and 5.0 times its normal value. Note transient alternation in *A*. Minimum value of Δt was decreased to 0.008 ms for this simulation to allow ΔV to remain <0.4 mV. *C* and *D*: period-doubling bifurcation in 3-dimensional system. As a parameter is changed, preexisting stable limit cycle (solid closed curve in *C*) becomes unstable (dashed curve in *D*) and spawns in its immediate vicinity a stable limit cycle (solid closed curve in *D*) that has twice the period of original stable limit-cycle oscillation in *C*.

Other biological oscillators. Although we have concentrated above on the SAN, our proposed classification scheme can be extended to include other cardiac oscillators. For example, the second way of stopping (annihilation) and the associated single-pulse triggering have been described in experiments on depolarized Purkinje fiber (38, 68; see other refs. in Ref. 20), depolarized ventricular muscle (24, 68), aggregates of embryonic atrial cells (72), the mitral valve (20), and in ionic models of the first three tissues (15, 16, 72, 80). In fact, a bifurcation diagram qualitatively equivalent to that shown in Fig. 6 can be obtained in a reduced two-dimensional model of ventricular muscle subjected to a depolarizing bias current (see Fig. 8 of Ref. 80). However, in the full ventricular model (16, 80) there is a subcritical rather than a supercritical Hopf bifurcation with depolarizing I_{bias}, leading to annihilation with the resting potential lying in the plateau, and not the pacemaker, range of potentials (see also Refs. 15, 43).

Patterns of activity resembling some of those shown in Fig. 9 can be seen in atrial muscle (64, 67), Purkinje fiber (see refs. in Ref. 27), and heart-cell aggregates (49), as well as in ionic models of the latter two tissues (Ref. 27 and J. R. Clay and A. Shrier, personal communication, respectively). However, unlike the case of the SAN, this modeling work shows that the existence of the maintained subthreshold oscillation and the skipped-beat runs, which occur in a more hyperpolarized range of potentials. hinges on the presence of I_h. A mirror image of the third way, in which there are afterpotentials in the plateau range of potentials ("early afterdepolarizations"), can be seen in Purkinje fiber and ventricular muscle and their models (15, 16, 18, 20, 80). In that case, the maintained small-amplitude oscillation ("I_x oscillation") lies in the plateau range of potentials, and the membrane becomes quiescent with the membrane potential lying in that range. In one of these modeling studies (16), the existence of chaotic dynamics was claimed. Two reports show that this inversion of the third way (i.e., early afterdepolarizations) can be seen in experiments on the SAN (50, 58).

Our classification scheme can be applied to biological oscillators originating from tissues other than the heart. For example, patterns of activity similar to those shown in Fig. 3, which are generated by a single Hopf bifurcation, have been described in the giant axon of the squid (2), as well as in the Hodgkin-Huxley equations that model the squid axon (2). Homoclinic orbits occur in the Hodgkin-Huxley equations when the Nernst potential for K^+ is changed in conjunction with injection of I_{bias} (42). Annihilation has been described experimentally in the squid axon (35), following its theoretical prediction in the Hodgkin-Huxley model (6, 35, 66). Skipped-beat runs [34 ("skip runs"), 45] and a maintained small-amplitude oscillation (45) have been described in neural tissue, as well as in an electronic analogue of the Hodgkin-Huxley equations (28). Skipped-beat runs (22) and a "slow-wave" subthreshold pacemaker oscillation are also commonly seen in smooth muscle.

Spatial effects. We have not dealt above with rhythms, such as sinoatrial exit block, intranodal reentry, or atrial fibrillation, in which the usual more-or-less concentric spread of activation out of the node and into the right atrium (7) is abolished and replaced by a different spatiotemporal organization of the activation sequence. Because propagation is involved, modeling of such rhythms involves simulation of a partial differential equation, and we have confined ourselves in the above to isopotential situations described by systems of ordinary differential equations. In addition, due to the highly complex nature of the coupling between cells in the SAN, it would be difficult to construct such a model in a realistic way, since, among other things, the usual cable-model approach used in such work would not be appropriate (e.g., see Fig. 4 of Ref. 8).

Clinical significance. Although injection of a single stimulus can indeed initiate nonsustained reentrant activity in a pathway including the SAN (3), Fig. 5*B* suggests that activity can also be initiated by a nonreentrant mechanism (see also discussion in chapt. VIII of Ref. 20). Figure 9, *B–D*, demonstrates a novel way of producing very long interbeat intervals. Should similar activity occur in the intact heart, analysis of the electrocardiogram would lead to the diagnosis of sinoatrial pause or exit block, even though the SAN would still be active, generating incrementing subthreshold prepotentials during the pause. Indeed in an arrhythmia that is presently diagnosed as one form of second-degree sinoatrial exit block (Wenckebach or Mobitz I), the prolonged R-R interval is less than twice the duration of the preceding R-R interval (77); similar rhythms can be seen at values of I_{bias} lying between those used in Fig. 9, *A* and *B*. In addition, should similar activity occur in a parasystolic focus [e.g., Purkinje fiber (27)], long interectopic intervals that would be approximately multiples of some basic interval would be manifest on the electrocardiogram. This would be attributed to intermittent exit block from the parasystolic focus, even though block of conduction would not be involved.

Nonlinear dynamics. In summary, consideration of a large body of experimental and modeling work in the SAN and other cardiac tissues points to the conclusion that the number of ways in which spontaneous activity in a cardiac oscillator can be stopped or started is quite small. In fact, the presently available experimental evidence indicates that this number might be as small as three in the SAN. It is not yet entirely clear why a particular intervention results in one way and not another. In particular, conditions necessary and sufficient for annihilation to occur are yet to be determined. Because annihilation can be seen in a reduced three-dimensional (V, f, p) version of the Irisawa-Noma model (33), we anticipate that further investigation of that model will help in sorting out these conditions. Finally, as in the case of periodically stimulated cardiac cells (e.g., see Ref. 29), the above work provides further evidence that concepts drawn from a branch of nonlinear mathematics, bifurcation theory, can be used to form a classification scheme for a variety of behaviors seen in experimental cardiac electrophysiology.

NOTE ADDED IN PROOF

Annihilation has been reported recently in an isolated SAN cell subjected to a depolarizing bias current (J. M. B. Anumonwo, et al. *Circ. Res.* 68: 1138–1153, 1991). Annihilation was not seen in the second cell studied, which was not subjected to a bias current.

We thank Dr. E. Doedel for providing us with the AUTO program, Dr. A. Vinet for help with installing AUTO, Dr. J. S. Outerbridge for use of the graphics package and general help with computers, Dr. A. van Ginneken for helpful comments on the manuscript, and Dr. H. Fozzard for directing us to the work of Teorell. We also thank Christine Pamplin and Sandra James for typing the manuscript, A. van Horssen for drafting some of the figures, and Robert Lamarche and Robert Thomson for photographing the figures.

M. R. Guevara, as a postdoctoral fellow, was supported by the Canadian Heart Foundation and the Natural Sciences and Engineering Research Council of Canada (1984–86). The study was supported by grants to H. J. Jongsma from the Dutch Organization for Pure Research and to M. R. Guevara from the Medical Research Council of Canada.

Present address of H. J. Jongsma: Fysiologisch Laboratorium, Universiteit van Amsterdam, Faculteit der Geneeskunde, Academisch Medisch Centrum, Meibergdreef 15, 1105 Amsterdam, The Netherlands.

Address for reprint requests: M. R. Guevara, Dept. of Physiology,

McGill University, 3655 Drummond St., Montreal, Quebec H3G 1Y6, Canada.

Received 19 September 1990; accepted in final form 27 November 1991.

REFERENCES

1. **Abraham, R. M., and C. D. Shaw.** *Dynamics—The Geometry of Behavior.* Santa Cruz, CA: Aerial, 1983, pt. 1–3.
2. **Aihara, K., and G. Matsumoto.** Temporally coherent organization and instabilities in squid giant axon. *J. Theor. Biol.* 95: 697–720, 1982.
3. **Allessie, M. A., and F. I. M. Bonke.** Direct demonstration of sinus node reentry in the rabbit heart. *Circ. Res.* 44: 557–568, 1979.
4. **Appelton, E. V., and B. van Der Pol, Jr.** On a type of oscillation-hysteresis in a simple triode generator. *Philos. Mag.* 43: 177–193, 1922.
5. **Argoul, F., A. Arneodo, P. Richetti, J. C. Roux, and H. L. Swinney.** Chemical chaos: from hints to confirmation. *Acc. Chem. Res.* 20: 436–442, 1987.
6. **Best, E. N.** Null space in the Hodgkin-Huxley equations. A critical test. *Biophys. J.* 27: 87–104, 1979.
7. **Bleeker, W. K., A. J. C. Mackaay, M. Masson-Pévet, L. N. Bouman, and A. E. Becker.** Functional and morphological organization of the rabbit sinus node. *Circ. Res.* 46: 11–22, 1980.
8. **Bouman, L. N., J. J. Duivenvoorden, F. F. Bukauskas, and H. J. Jongsma.** Anisotropy of electrotonus in the sinoatrial node of the rabbit heart. *J. Mol. Cell. Cardiol.* 21: 407–418, 1989.
9. **Bozler, E.** The initiation of impulses in cardiac muscle. *Am. J. Physiol.* 138: 273–282, 1943.
10. **Brooks, C. M., and H.-H. Lu.** *The Sinoatrial Pacemaker of the Heart.* Springfield, IL: Thomas, 1972.
11. **Brown, H., J. Kimura, and S. Noble.** The relative contributions of various time-dependent membrane currents to pacemaker activity in the sino atrial node. In: *Cardiac Rate and Rhythm*, edited by L. N. Bouman and H. J. Jongsma. The Hague: Nijhoff, 1982, p. 54–68.
12. **Brown, H. F., J. Kimura, D. Noble, S. J. Noble, and A. Taupignon.** The ionic currents underlying pacemaker activity in rabbit sino-atrial node: experimental results and computer simulations. *Proc. R. Soc. Lond. B Biol. Sci.* 222: 329–347, 1984.
13. **Brown, H. F., D. Noble, S. J. Noble, and A. I. Taupignon.** Relationship between the transient inward current and slow inward currents in the sino-atrial node of the rabbit. *J. Physiol. Lond.* 370: 299–315, 1986.
14. **Chandler, W. K., R. Fitzhugh, and K. S. Cole.** Theoretical stability properties of a space-clamped axon. *Biophys. J.* 2: 105–127, 1962.
15. **Chay, T. R., and Y. S. Lee.** Impulse responses of automaticity in the Purkinje fiber. *Biophys. J.* 45: 841–849, 1984.
16. **Chay, T. R., and Y. S. Lee.** Phase resetting and bifurcation in the ventricular myocardium. *Biophys. J.* 47: 641–651, 1985.
17. **Clay, J. R., M. R. Guevara, and A. Shrier.** Phase resetting of the rhythmic activity of embryonic heart cell aggregates. Experiment and theory. *Biophys. J.* 45: 699–714, 1984.
18. **Cranefield, P. F.** Action potentials, afterpotentials and arrhythmias. *Circ. Res.* 41: 415–423, 1977.
19. **Cranefield, P. F.** Does spontaneous activity arise from phase 4 depolarization or from triggering? In: *The Sinus Node*, edited by F. I. M. Bonke. The Hague: Nijhoff, 1978, p. 348–356.
20. **Cranefield, P. F., and R. S. Aronson.** *Cardiac Arrhythmias: The Role of Triggered Activity and Other Mechanisms.* Mount Kisco, NY: Futura, 1988.
21. **Doedel, E. J., and J. P. Kernevez.** *Software for Continuation Problems in Ordinary Differential Equations With Applications.* Pasadena: California Institute of Technology, 1986. (Technical Report, Applied Mathematics)
22. **Droogmans, G., and G. Callewaert.** Ca^{++}-channel current and its modification by the dihydropyridine agonist BAY k 8644 in isolated smooth muscle cells. *Pfluegers Arch.* 406: 259–265, 1986.
23. **Gaspard, P., R. Kapral, and G. Nicolis.** Bifurcation phenomena near homoclinic systems: a two-parameter analysis. *J. Stat. Phys.* 35: 697–727, 1984.
24. **Gilmour, R. F., Jr., J. J. Heger, E. N. Prystowsky, and D. P. Zipes.** Cellular electrophysiologic abnormalities of diseased human ventricular myocardium. *Am. J. Cardiol.* 51: 137–144, 1983.
25. **Glass, L., and M. C. Mackey.** *From Clocks to Chaos: The Rhythms of Life.* Princeton, NJ: Princeton Univ. Press, 1988.
26. **Glendinning, P., and C. Sparrow.** Local and global behaviour near homoclinic orbits. *J. Stat. Phys.* 35: 645–695, 1984.
27. **Guevara, M. R.** Afterpotentials and pacemaker oscillations in an ionic model of cardiac Purkinje fibres. In: *Temporal Disorder in Human Oscillatory Systems*, edited by L. Rensing, U. an der Heiden, and M. C. Mackey. Berlin: Springer, 1987, p. 127–133.
28. **Guevara, M. R.** Displaced reinjection attractors in an electronic analogue of the membrane of the squid giant axon. In: *A Chaotic Hierarchy*, edited by M. Klein and G. Baier. Singapore: World Scientific, 1991, p. 153–164.
29. **Guevara, M. R., L. Glass, and A. Shrier.** Phase locking, period-doubling bifurcations, and irregular dynamics in periodically stimulated cardiac cells. *Science Wash. DC* 214: 1350–1353, 1981.
30. **Guevara, M. R., and H. J. Jongsma.** Phase resetting in a model of sinoatrial nodal membrane: ionic and topological aspects. *Am. J. Physiol.* 258 (*Heart Circ. Physiol.* 27): H734–H747, 1990.
31. **Guevara, M. R., and A. Shrier.** Phase resetting in a model of cardiac Purkinje fiber. *Biophys. J.* 52: 165–175, 1987.
32. **Guevara, M. R., A. Shrier, and L. Glass.** Phase resetting of spontaneously beating embryonic ventricular heart cell aggregates. *Am. J. Physiol.* 251 (*Heart Circ. Physiol.* 20): H1298–H1305, 1986.
33. **Guevara, M. R., A. C. G. van Ginneken, and H. J. Jongsma.** Patterns of activity in a reduced ionic model of a cell from the rabbit sinoatrial node. In: *Chaos in Biological Systems*, edited by H. Degn, A. V. Holden, and L. F. Olsen. London: Plenum, 1987, p. 5–12.
34. **Guttman, R., and R. Barnhill.** Oscillation and repetitive firing in squid axons. *J. Gen. Physiol.* 55: 104–118, 1970.
35. **Guttman, R., S. Lewis, and J. Rinzel.** Control of repetitive firing in squid axon membrane as a model for a neuroneoscillator. *J. Physiol. Lond.* 305: 377–395, 1980.
36. **Irisawa, H., and A. Noma.** Pacemaker mechanisms of rabbit sinoatrial node cells. In: *Cardiac Rate and Rhythm*, edited by L. N. Bouman and H. J. Jongsma. The Hague: Nijhoff, 1982, p. 35–51.
37. **Jalife, J., and C. Antzelevitch.** Phase resetting and annihilation of pacemaker activity in cardiac tissue. *Science Wash. DC* 206: 695–697, 1979.
38. **Jalife, J., and C. Antzelevitch.** Pacemaker annihilation: diagnostic and therapeutic implications. *Am. Heart J.* 100: 128–130, 1980.
39. **Kodama, I., and M. R. Boyett.** Regional differences in the electrical activity of the rabbit sinus node. *Pfluegers Arch.* 404: 214–226, 1985.
40. **Kohlhardt, M., H.-R. Figulla, and O. Tripathi.** The slow membrane channel as the predominant mediator of the excitation process of the sinoatrial pacemaker cell. *Basic Res. Cardiol.* 71: 17–26, 1976.
41. **Kreitner, D.** Electrophysiological study of the two main pacemaker mechanisms in the rabbit sinus node. *Cardiovasc. Res.* 19: 304–318, 1985.
42. **Labouriau, I. S.** Homoclinic and periodic solutions of nerve impulse equations. In: *Chaos in Biological Systems*, edited by H. Degn, A. V. Holden, and L. F. Olsen. London: Plenum, 1987, p. 105–111.
43. **Landau, M., P. Lorente, D. Michaels, and J. Jalife.** Bistabilities and annihilation phenomena in electrophysiological cardiac models. *Circ. Res.* 66: 1658–1672, 1990.
44. **Lipsius, S. L.** Electrotonic interactions in delayed propagation and block within the guinea pig SA node. *Am. J. Physiol.* 245 (*Heart Circ. Physiol.* 14): H7–H16, 1983.
45. **Llinas, R., and Y. Yarom.** Oscillatory properties of guinea-pig inferior olivary neurones and their pharmacological modulation: an in vitro study. *J. Physiol. Lond.* 376: 163–182, 1986.
46. **Maselko, J., and H. L. Swinney.** A complex transition sequence in the Belousov-Zhabotinskii reaction. *Phys. Scr.* T9: 35–39, 1985.
47. **Mauro, A., F. Conti, F. Dodge, and R. Schor.** Subthreshold behaviour and phenomenological impedance of the squid giant axon. *J. Gen. Physiol.* 55: 497–523, 1970.
48. **Maylie, J., and M. Morad.** Ionic currents responsible for the generation of pace-maker current in the rabbit sino-atrial node. *J. Physiol. Lond.* 355: 215–235, 1984.
49. **McDonald, T. F., and H. G. Sachs.** Electrical activity in embryonic heart cell aggregates. *Pfluegers Arch.* 354: 165–176, 1975.
50. **Miyamae, S., and K. Goto.** The effects of extracellular calcium removal on sino-atrial node cells treated with potassium-depleted solutions. *Jpn. J. Physiol.* 36: 403–409, 1986.

51. **Nilius, B.** Possible functional significance of a novel type of cardiac Ca channel. *Biomed. Biochim. Acta* 45: K37–K45, 1986.
52. **Noble, D., and S. J. Noble.** A model of sino-atrial node electrical activity based on a modification of the DiFrancesco-Noble (1984) equations. *Proc. R. Soc. Lond. B Biol. Sci.* 222: 295–304, 1984.
53. **Noma, A.** Mechanisms underlying cessation of rabbit sinoatrial node pacemaker activity in high potassium solutions. *Jpn. J. Physiol.* 26: 619–630, 1976.
54. **Noma, A., and H. Irisawa.** Electrogenic sodium pump in rabbit sinoatrial node cell. *Pfluegers Arch.* 351: 177–182, 1974.
55. **Noma, A., and H. Irisawa.** The effect of sodium ion on the initial phase of the sinoatrial pacemaker action potential in rabbits. *Jpn. J. Physiol.* 24: 617–632, 1974.
56. **Noma, A., and H. Irisawa.** Effects of Na^+ and K^+ on the resting membrane potential of the rabbit sinoatrial node cell. *Jpn. J. Physiol.* 25: 287–302, 1975.
57. **Noma, A., M. Morad, and H. Irisawa.** Does the "pacemaker current" generate the diastolic depolarization in the rabbit SA node cells? *Pfluegers Arch.* 397: 190–194, 1983.
58. **Ohba, M.** Effects of tonicity on the pacemaker activity of guinea-pig sino-atrial node. *Jpn. J. Physiol.* 36: 1027–1038, 1986.
59. **Oei, H. I., A. C. G. van Ginneken, H. J. Jongsma, and L. N. Bouman.** Mechanisms of impulse generation in isolated cells from the rabbit sinoatrial node. *J. Mol. Cell. Cardiol.* 21: 1137–1149, 1989.
60. **Opthof, T., B. de Jonge, M. Masson-Pevet, H. J. Jongsma, and L. N. Bouman.** Functional and morphological organization of the cat sinoatrial node. *J. Mol. Cell. Cardiol.* 18: 1015–1031, 1986.
61. **Opthof, T., A. C. G. van Ginneken, L. N. Bouman, and H. J. Jongsma.** The intrinsic cycle length in small pieces from the rabbit sinoatrial node. *J. Mol. Cell Cardiol.* 19: 923–934, 1987.
62. **Osterrieder, W., D. Pelzer, Q.-F. Yang, and W. Trautwein.** The electrophysiological basis of the bradycardic action of AQA 39 on the sinoatrial node. *Naunyn-Schmiedeberg's Arch. Pharmacol.* 317: 233–237, 1981.
63. **Osterrieder, W., Q.-F. Yang, and W. Trautwein.** Effects of barium on the membrane currents in the rabbit S-A node. *Pfluegers Arch.* 394: 78–84, 1982.
64. **Paes de Carvalho, A.** Slow and subliminal responses: their mechanism and relationship to other oscillatory phenomena in cardiac muscle. In: *Cardiac Electrophysiology and Arrhythmias*, edited by D. P. Zipes and J. Jalife. Orlando, FL: Grune & Stratton, 1985, p. 89–96.
65. **Reiner, V. S., and C. Antzelevitch.** Phase resetting and annihilation in a mathematical model of sinus node. *Am. J. Physiol.* 249 (*Heart Circ. Physiol.* 18): H1143–H1153, 1985.
66. **Rinzel, J., and R. N. Miller.** Numerical calculation of stable and unstable periodic solutions to the Hodgkin-Huxley equations. *Math. Biosci.* 49: 27–59, 1980.
67. **Rosen, M. R., and A. J. Hordof.** The slow response in human atrium. In: *The Slow Inward Current and Cardiac Arrhythmias*, edited by D. P. Zipes, J. C. Bailey, and V. Elharrar. The Hague: Nijhoff, 1980, p. 295–308.
68. **Rosenthal, J. E., and G. R. Ferrier.** Contribution of variable entrance and exit block in protected foci to arrhythmogenesis in isolated ventricular tissues. *Circulation* 67: 1–8, 1983.
69. **Sanguinetti, M. C., and T. C. West.** Influence of papaverine on spontaneous activity of isolated right atria from small mammals. *J. Pharmacol. Exp. Ther.* 228: 500–509, 1984.
70. **Senami, M., and H. Irisawa.** Effect of procaine amide on the membrane currents of the sino-atrial node cells of rabbits. *Jpn. J. Physiol.* 31: 225–236, 1981.
71. **Seydel, R.** *From Equilibrium to Chaos: Practical Bifurcation and Stability Analysis.* Amsterdam: Elsevier, 1988.
72. **Shrier, A., J. R. Clay, and R. Brochu.** Effects of tetrodotoxin on heart cell aggregates. Phase resetting and annihilation of activity. *Biophys. J.* 58: 623–629, 1990.
73. **Teorell, T.** A biophysical analysis of mechano-electrical transduction. In: *Principles of Receptor Physiology*, edited by W. R. Loewenstein. Berlin: Springer, 1971, vol. 1, p. 291–339.
74. **Thompson, J. M. T., and H. B. Stewart.** *Nonlinear Dynamics and Chaos.* Chichester, UK: Wiley, 1986.
75. **Trautwein, W.** Effect of acetylcholine on the S-A node of the heart. In: *Cellular Pacemakers*, edited by D. O. Carpenter. New York: Wiley, 1982, vol. 1, p. 127–160.
76. **Tuganowski, W., M. Krause, and K. Korczak.** The effect of dibutyryl 3′5′-cyclic AMP on the cardiac pacemaker, arrested with reserpine and α-methyl-tyrosine. *Naunyn-Schmiedeberg's Arch. Pharmacol.* 280: 63–70, 1973.
77. **Vaiciulyte, R., and J. Kaukenas.** Clinical and computer diagnosis of the second degree sinoauricular block by the method of rhythmography. In: *Electrophysiology and Surgery of Cardiac Arrhythmias*, edited by J. Bredikis. Vilnius: Mokslas, 1987, p. 102–108.
78. **Van Meerwijk, W. P. M., G. de Bruin, A. C. G. van Ginneken, J. van Hartevelt, H. J. Jongsma, E. W. Kruyt, S. S. Scott, and D. L. Ypey.** Phase resetting properties of cardiac pacemaker cells. *Biophys. J.* 83: 613–629, 1984.
79. **Victorri, B., A. Vinet, F. A. Roberge, and J.-P. Drouhard.** Numerical integration in the reconstruction of cardiac action potentials using Hodgkin-Huxley-type models. *Comp. Biomed. Res.* 18: 20–23, 1985.
80. **Vinet, A., and F. A. Roberge.** A model study of stability and oscillations in the myocardial cell membrane. *J. Theor. Biol.* 147: 377–412, 1990.
81. **West, T. C.** Effects of chronotropic influences on subthreshold oscillations in the sino-atrial node. In: *The Specialized Tissues of the Heart*, edited by A. Paes de Carvalho, W. C. de Mello, and B. F. Hoffman. Amsterdam: Elsevier, 1961, p. 81–94.
82. **Wiggins, S.** *Global Bifurcation and Chaos. Analytical Methods.* New York: Springer, 1988.
83. **Winfree, A. T.** Phase control of neural pacemakers. *Science Wash. DC* 197: 761–763, 1977.
84. **Winfree, A. T.** *When Time Breaks Down: The Three-Dimensional Dynamics of Electrochemical Waves and Cardiac Arrhythmias.* Princeton, NJ: Princeton Univ. Press, 1987.
85. **Woods, W. T., F. Urthaler, and T. N. James.** Electrical activity in canine sinus node cells during arrest produced by acetylcholine. *J. Mol. Cell. Cardiol.* 13: 349–357, 1981.
86. **Yanagihara, K., A. Noma, and H. Irisawa.** Reconstruction of sino-atrial node pacemaker potential based on the voltage clamp experiments. *Jpn. J. Physiol.* 30: 841–857, 1980.